Thesis for The Degree of Licentiate of Engineering

Superconducting THz mixers based on MgB_2 film

Stella Bevilacqua

Terahertz and Millimetre Wave Laboratory
Department of Microtechnology and Nanoscience - MC2
Chalmers University of Technology
Göteborg, Sweden 2013

Superconducting THz mixers based on MgB_2 film

Stella Bevilacqua

Terahertz and Millimetre Wave Laboratory
Department of Microtechnology and Nanoscience - MC2
Chalmers University of Technology
SE-412 96 Göteborg, Sweden
Phone: +46 (0) 31 772 1000

Technical Report MC2-239
ISSN 1652-0769

Cover: Hot electron bolometer integrated with spiral antenna

Printed by Chalmers Reproservice
Göteborg, Sweden, 2013

A Giuseppe, mamma e papà

Abstract

Superconducting NbN hot electron bolometer (HEB) mixers are widely used in terahertz radio astronomy. Such mixers have superior performance compared to SIS and Schottky diode mixers at frequency above 1 THz. However, their drawback is a limited IF bandwidth. Therefore, as radio astronomy advances towards higher frequencies, mixers with even wider gain bandwidth are required. The gain bandwidth of the HEB mixers is determined by two consequent processes in the electron energy relaxation: the electron phonon interaction and the phonon escape into the substrate with corresponding time constants for each process. The electron-phonon interaction time is inversely dependent of the electron temperature of the film which is close to the critical temperature of the superconductor. The escape time is dependent of the film thickness. Materials with higher critical temperature and shorter electron relaxation time are needed to improve the IF bandwidth.

The discovery of the superconductivity in the intermetallic compound magnesium diboride (MgB_2) has generated a great interest in this research field. The high critical temperature and the short electron phonon interaction time make the MgB_2 very attractive for HEB mixers fabrication aiming for better HEB mixers performances.

In this thesis, novel terahertz HEB mixers based on magnesium diboride thin films are presented. MgB_2 HEBs integrated with spiral antenna were fabricated, characterized and studied. The gain bandwidth was investigated with respect to the thickness and the critical temperature of the film. A gain bandwidth of 1.3 GHz, 2.3 GHz and 3.4 GHz corresponding to a mixer time constant of 130 ps, 70 ps and 47 ps was measured in 30 nm, 15 nm and 10 nm MgB_2 films, respectively. Another important figure of merit for receivers is the noise temperature which is influenced by several factors such as the dimension of the HEB and the critical current. For HEB mixers made from 10 nm MgB_2 film the lowest mixer noise temperature was 600 K measured at 2 K bath temperature and 600 GHz local oscillator (LO) frequency. Finally, using the two temperature model the experimental data were analyzed and the electron phonon interaction time, τ_{e-ph} of 7 to 15 ps, the phonon escape time, τ_{esc} of 6 to 42 ps and the specific heat ratio, c_e/c_{ph} of 1.35 to 9 ps were extracting giving the first model for HEB mixers made of MgB_2 films. Based on this research a gain bandwidth as large as 8-10 GHz has been predicted in very thin MgB_2 films.

Keywords: THz Detectors, bolometers, mixers, MgB_2, superconductors, IF bandwidth.

List of Publications

Appended papers

This thesis is based on the following papers:

[A] S. Bevilacqua, S. Cherednichenko, V. Drakinskiy, H. Shibata, A. Hammar and J. Stake "Investigation of MgB_2 HEB mixer gain bandwidth", in *IEEE International Conference on Infrared, Millimeter and Terahertz Waves*, pp. 1-2, 2-7 October 2011, Houston.

[B] S. Bevilacqua, S. Cherednichenko, V. Drakinskiy, J. Stake, H. Shibata and Y.Tokura "Low noise MgB_2 terahertz hot-electron bolometer", in *Applied Physics Letter*, vol.100, no.3, pp.033504-033504-3, January 2012.

[C] S. Bevilacqua, S. Cherednichenko, V. Drakinskiy, H. Shibata, Y.Tokura and J. Stake "Study of IF Bandwidth of MgB_2 Phonon-cooled Hot-electron bolometer mixers", submitted to *IEEE Transactions on Terahertz Science and Technology*, 2012.

Other papers and publications

The following papers and publications are not appended to the thesis, either due to contents overlapping of that of appended papers, or due to contents not related to the thesis.

[a] A. Hammar, S. Cherednichenko, **S. Bevilacqua**, V. Drakinskiy and J. Stake, "Terahertz Direct Detection in $YB_{a2}Cu_3O_7$", *IEEE Transactions on Terahertz Science and Technology*, vol.1, no.2, pp.390-394, November 2011.

[b] S. Cherednichenko, A. Hammar, **S. Bevilacqua**, V. Drakinskiy, J. Stake, Alexey Kalabukhov, "A Room Temperature Bolometer for Terahertz Coherent and Incoherent Detection", *IEEE Transactions on Terahertz Science and Technology*, vol.1, no.2, pp.395-402, November 2011.

Notations and abbreviations

Notations

A	Area
β	Acoustic phonon transmission coefficient
α	Temperature Coefficient of Resistance
c	Speed of light
C	Heat Capacitance
C_0	Self heating parameter
c_e	Electron specific heat
c_{ph}	Phonon specific heat
d	Material thickness
D	Electron diffusivity
Δ	Energy gap
ΔP	Power variation
$\Delta\Theta_{IF}$	Amplitude of the response
ΔT_C	Transition width
$\Delta T(\omega)$	Temperature modulation
ΔV	Voltage variation
E	Energy
ε_0	Vacuum permittivity
f	Frequency
f_g	Gain bandwidth frequency
f_{IF}	Intermediate frequency
f_{LO}	Local oscillator frequency
f_n	Noise bandwidth frequency
f_s	Signal frequency
G	Thermal conductance
G_e	Effective Thermal conductance
γ	Electron phonon specific heat coefficient
h	Planck´s constant
η_m	Mixer gain
H_C	Critical magnetic field
k_B	Boltzmann´s constant

I	Current
I_C	Critical current
L_{th}	Thermal diffusion length
λ	Wavelength
λ_L	London penetration depth
m	Mass
M	Molar mass
n	Superconducting electron density
NEP	Noise equivalent power
n_a	Atomic mass density
ξ	Coherence length
P	Power
P_{IF}	Intermediate power
P_{LO}	Local oscillator power
P_S	Signal power
$P(\omega)$	Power modulation
R	Resistance
R_{bd}	Boundary Resistance
R_d	Differential Resistance
R_L	Load Resistance
R_0	Bias resistance
ρ	Resistivity
ρ_m	Mass density
S_v	Responsivity
T	Temperature
T_B	Bolometer temperature
T_{bath}	Reservoir temperature
T_c	Critical temperature
T_D	Debye temperature
T_e	Electron temperature
T_{IF}	Amplifier noise temperature
T_{ph}	Phonon temperature
T_{TFn}	Thermal fluctuation noise
T_{rec}	Receiver noise temperature
T_{Jn}	Johnson noise
τ	Time constant
τ_θ	Response time
τ_e	Electron cooling time
τ_{e-ph}	Electron phonon interaction time
τ_{esc}	Phonon escape time
τ_{diff}	Diffusion time
u	Speed of sound
V	Voltage
v_F	Fermi velocity
V_{LO}	Voltage amplitude of the local oscillator
V_S	Voltage amplitude of the signal
ω	Angular frequency
ω_{IF}	Intermediate angular frequency
ω_{LO}	Local oscillator angular frequency
ω_S	Signal angular frequency

Abbreviations

Au	Gold
BWO	Backward wave oscilaltor
DSB	Double sideband
FET	Field effect transistor
FIB-SEM	Focused ion beam scanning electron microscope
FIR	Far Infrared
GBW	Gain bandwidth
GHz	10^9 Hz
HEB	Hot electron bolometer
IF	Intermediate frequency
InSb	Indium antimonide
LHe	Liquid helium
LNA	Low noise amplifier
LO	Local oscillator
LSB	Lower sideband
MBE	Molecular beam epitaxy
MgB_2	Magnesium diboride
MHz	10^6 Hz
Nb	Niobium
Nb_3Ge	Niobium germanium
NbN	Niobium nitride
NBW	Noise bandwidth
NbTiN	Niobium titanium nitride
RF	Radio frequency
SD	Schottky diode
SEM	Scanning electron microscope
SiN_x	Silicon Nitride
SIS	Superconductor insulator tunnel junction
SSB	Single sideband
2SB	Sideband separating
TCR	Temperature coefficient of resistance
THz	10^{12} Hz
Ti	Titamium
USB	Upper sideband

Contents

Abstract **v**

List of Publications **vii**

Notations and abbreviations **ix**

1 Introduction **1**
1.1 THz mixers 1
1.2 Motivation of the thesis 4
1.3 Thesis overview 5

2 Background **7**
2.1 Bolometer description 7
2.2 Bolometric detector 9
2.2.1 Direct detection 9
2.2.2 Heterodyne mixing 12
2.3 Hot electron bolometer mixers 17
2.4 Basics of superconductivity 18
2.4.1 Magnesium diboride films MgB_2 20

3 MgB_2 HEB fabrication process and DC characterisation **23**
3.1 UV-Lithography process 23
3.2 Electron beam lithography process 26
3.3 DC characterisation 28

4 THz characterisation and discussion **33**
4.1 Experimental technique 33
4.2 Results 35
4.3 Two-temperature model 39

5 Conclusions and future work **43**

6 Summary of appended papers **45**

Acknowledgments **47**

Bibliography **49**

Appended Papers **57**

Chapter 1

Introduction

The electromagnetic spectrum between the microwave (0.1 THz; $\lambda \sim 3\,\mathrm{mm}$) and the Infrared frequencies (10 THz; $\lambda \sim 30\,\mu\mathrm{m}$) is identified as the terahertz (THz) region [1]. THz technology is applied to numerous fields such as high-resolution radar system, medical and biological imaging and probing [2], Earth environment, security and communication. THz detectors are strongly needed in radio astronomy; indeed one-half of the total luminosity of the Universe and 98% of the photons emitted since the Big Bang fall into the Far-Infrared (FIR) and submillimetre range [1]. This region of the electromagnetic spectrum is not fully explored due to the difficulties to built high output power sources and receivers. Moreover in this frequency range there is a significant attenuation of the useful signal due to the absorption of the radiation in the Earth atmosphere. In order to reduce such losses, THz observatories are placed on high mountains or are using balloons, airplanes or satellite in Space. The exploration of the submillimetre wave range leads to important information about development of galaxies, star formation and origin of the chemical elements in Space. Furthermore, THz radiation is used to explore the atmospheres of comets and planets as well as the cosmic background radiation originating in the "early years" after the Big Bang. Radio astronomical facilities such as the ALMA interferometer [3], the APEX telescope [4], the Herschel Space Observatory [5], COBE [6] and many others are used to explore various aspects of the universe (see fig:1.1). These THz radiation observation platforms require detectors with high sensitivity and large bandwidth [7]. Today, heterodyne receivers used in high spectral resolution radio astronomy are based on cryogenic devices such as insulator-superconductor tunnel junctions (SIS) and hot electron bolometers (HEB). The use of those devices is motivated by the superior sensitivity and low local oscillator (LO) power compared to e.g Schottky diode technology. Table 1.1 shows the state of the art of some THz detectors and their operation frequency range.

1.1 THz mixers

Detection systems in the THz spectral range can be divided in two classes: direct (incoherent) detectors and heterodyne (coherent) detectors. In the direct detection mode the power received by the detecting devices is measured in a

Fig. 1.1: Illustrations of several radio astronomical platforms. The Herschel Space Observatory [5], the APEX telescope [4], the ALMA interferometer [3] and COBE [6].

Table 1.1: Frequency operation of THz detectors. Microbolometer [8–10], HEB [11–16], SIS [17–19], SD [7, 20–22], FET [23, 24].

Detector	Operation frequency (THz)	Detection Type
microbolometer	0.3-30	incoherent detection
HEB	0.8-2.55	incoherent detection
HEB	0.3-5.25	coherent detection
SIS	0.14-0.25	incoherent detection
SIS	0.085-1.2	coherent detection
SD	0.1-2	incoherent detection
SD	0.085-5	coherent detection
FET	0.7	incoherent detection
FET	0.2-4.3	coherent detection

wide frequency range. Incoherent detectors allow only signal amplitude detection without preserving the phase information of the incoming signal. Such detectors are suitable for studying broadband radiation where high spectral resolution is not a requirement. Unlike incoherent detectors, coherent detectors preserve both the amplitude and the phase of the incoming radiation and they are used to characterize the signal with very high spectral resolution. In the heterodyne detection mode the RF signal f_S to be detected (e.g. a molecular line from a distant galaxy) is mixed with a strong local oscillator (LO) at frequency f_{LO} and downconverted to an intermediate frequency f_{IF} which is then amplified and detected by e.g. a spectrum analyzer. In the heterodyne detection the detecting device is used as a mixer. Different types of detectors are employed at THz frequencies such as Schottky diodes (SD), superconductor-insulator-superconductor (SIS) tunnel junctions, superconducting hot electron bolometer (HEB), Golay cells, field effect transistor (FET) and semiconductor bolometer. In this section, three types of detectors that are commonly employed in high sensitivity THz heterodyne receivers are briefly compared.

Schottky diodes are the most sensitive room temperature THz mixers. However, these receivers require a large amount of local oscillator power (LO) ($\sim$mW) at f>1THz [25], making it necessary to use large gas laser as local oscillator, rather unpractical condition for space-borne observations.

Their main advantages is that they have wide bandwidth and they can operate in a wide temperature range and therefore they can be used when cryogenic cooling is not possible or too expensive.

For frequencies below 1 THz, superconductor insulator superconductor (SIS) tunnel junctions based on Nb (niobium) are the most sensitive THz mixers. An additional advantage is their modest LO power requirement which is on the order of microwatts. The major drawback for SIS mixers is that the upper operating frequency is limited due to the superconducting gap frequency (700 GHz for Nb and about 1400 GHz for NbTiN) [26, 27]. At frequencies beyond the gap frequency (f=2Δ/h [7]), the photon assisted tunneling is limited. Another limitation comes from the material of the tuning circuit used to compensate for the SIS junction capacitance. If it is made from a superconductor, losses increase above the energy gap with the consequence of decreasing the receiver sensitivity. Alternative materials, such as NbN, NbTiN and Al, have been used instead of Nb to increase the operation frequency up to 1.2 THz [18].

An alternative to terahertz SIS mixers at frequency above 1.2 THz, that has received great interest from the research field, is the superconducting hot electron bolometer (HEB) mixer. Although HEB mixers provide smaller IF bandwidth compared to Schottky diode and SIS mixers, nevertheless the high sensitivity and the low LO power requirement ($<1\mu$W) [28], have determined the choice of HEB mixers for several ground and Space based observatories at THz frequencies [1].

The figure of merit, which define the sensitivity of THz mixers is the noise temperature. Figure 1.2 shows an overview of the double sideband (DSB) noise temperature versus frequency for Schottky, SIS and HEB mixers. The drawbacks of cooled versus room temperature technology are the high complexity of the equipments used as well as the limited lifetime which is restricted by the amount of the cooling agent (LHe). The type of technologies depend of

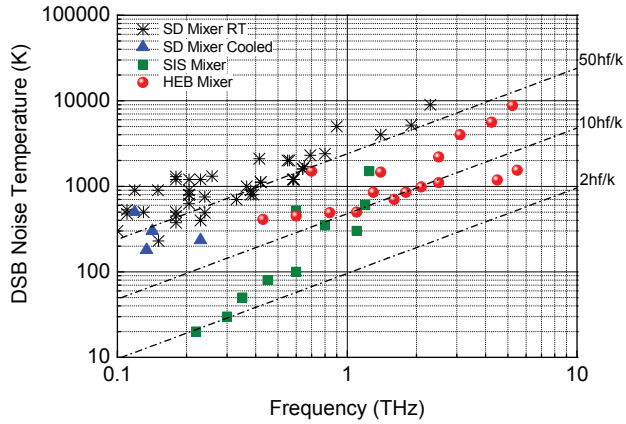

Fig. 1.2: State of the art performance of terahertz mixers. Room temperature and cooled Schottky diode mixer [7, 28–35], SIS mixer [28] and HEB mixer [13, 28].

the applications. In astrophysics cooled receivers are needed whereas portable systems and uncooled receivers are preferable for spectroscopy and imaging applications.

1.2 Motivation of the thesis

This section is focused on the superconducting phonon-cooled hot electron bolometer which is the detector type used in this research. In particular the motivations of this thesis are presented.

When the HEB is used in a THz mixer, it has to be fast enough to yield a useful IF bandwidth of a few GHz. The first HEB mixer was made from semiconducting InSb [36], which despite of having good noise performance, the bandwidth was just 1 MHz. Other semiconducting materials have been proposed for HEB fabrication [11, 37] but the long response time of semiconducting compared to superconducting HEBs make them suitable for direct detection but not for mixers.

Hot electron bolometer made from superconducting materials can work according to two mechanisms. Phonon-cooled and diffusion cooled mechanisms.

In Phonon-cooled HEB mixers, the gain bandwidth (GBW) is determined by two consequent processes in the electron energy relaxation: the electron-phonon interaction and the phonon energy interaction. The electron-phonon interaction time is inversely dependent on the critical temperature of the superconducting film, T_c, whereas the phonon-escape time depends on the film thickness. HEB mixers made of ultrathin 3-4 nm NbN film have demonstrated superior performance over other type of mixers (e.g. Schottky and SIS mixers) at frequencies above 1.2 THz [7, 13, 38]. The gain bandwidth was 3-4 GHz for 3-4 nm film [28] which is good enough for many radio astronomy applications. Further reduction of the NbN film thickness (less than 3-4 nm) leads to a drastic reduction of the critical temperature which acts towards the reduction of the

GBW [39]. Therefore, increasing the GBW of phonon-cooled NbN HEB mixers beyond the presently achieved 3-4 GHz seem to be unrealistic. A possible method to extend the gain bandwidth is to use diffusion-cooled HEB mixers, where an extra electron cooling path occurs by out-diffusion of the electrons in to the contact pads. A gain bandwidth as large as 1.7 GHz and 6.5 GHz has been demonstrate for Nb [40] and NbN HEB [41] mixers respectively. Such mixers require to be extremely short, as well as special treatment of the contact pads [42]. In order to increase the gain bandwidth of phonon-cooled HEB mixers an alternative is to search for superconducting materials with a faster response. The superconductivity in magnesium diboride was discovered by Akimitsu´s group in 2001 [43]. An high critical temperature (39 K) in the bulk, makes it very attractive to replace NbN with MgB_2, aiming for a better HEB mixer performances. Indeed, using superconducting film with a higher operating temperature is expected a reduction of the electron-phonon interaction time [44]. A larger gain bandwidth can be reached in a superconducting film with higher critical temperature. Moreover, it has been demonstrated that even thin (7.5 nm) MgB_2 film can exhibit a critical temperature as high as 34 K [45]. Using time domain spectroscopy the electron-phonon interaction time as been measured to be shorter in a thin MgB_2 film (3 ps at 39 K [46]) compared to NbN film (12 ps [47] at 10 K). The wider operating temperature range of MgB_2 compared to NbN makes it suitable for low noise and wide GBW mixers. In principle, HEBs based on MgB_2 are expected to operate faster than NbN counterparts.

The motivation of the research presented in this thesis is the study of new class of THz phonon-cooled hot electron bolometer mixers based of magnesium diboride (MgB_2) film. Achievement of the gain bandwidth (as well as of the noise bandwidth) superior to the NbN HEB mixers is the main goal of this work.

In this thesis, MgB_2 phonon-cooled HEB mixers were designed, fabricated and characterized. Beside to the demonstration of competitive performances of this new type of mixers with the existing technologies, the other goal was to get a reproducible and reliable fabrication process since the film was very sensitive to the water and oxygen. The RF characterisation of the MgB_2 HEB mixers was mainly done at 0.6 THz. In order to understand the superconductor response on a RF radiation the devices were analysed using the two-temperature model. Based on these results, on the material parameters and on the two-temperature model a GBW as large as 8-10 GHz is predicted for very thin MgB_2 film. Therefore, MgB_2 thin films appear very promising for low noise and wide GBW mixers for THz radio astronomy, as well as in other applications requiring broadband THz mixers.

1.3 Thesis overview

The thesis is structured in 4 chapters. Chapter 1, gives an introduction about THz detection and existing technologies for radio astronomy and Space science. Moreover the motivations of this research are presented. Chapter 2 concerns the detailed description of HEBs working principle, heterodyne mixing and basics of superconductivity. The HEBs fabrication process is described in

chapter 3. The experimental results are presented in chapter 4 with a detailed description of the measurement setups. Finally in chapter 5 a summary of this work and a description of future work are discussed.

Chapter 2

Background

This chapter provides an overview about the bolometer operation as well as the important figure of merits which determine the performance of a bolometer. Two ways to detect radiation, direct and heterodyne detection, are presented and discussed. Finally, theory about superconductivity and properties of magnesium diboride superconductor are given.

2.1 Bolometer description

A bolometer is a thermal detector that is used to measure power of the incident electromagnetic radiation. The bolometer can be made of superconducting, semiconducting, intermetallic or metals materials [48]. Figure 2.1 shows schematically the temperature dependence of resistance of different material types used for making bolometer. A simplified schematics of a bolometer which consists of an absorber with heat capacity C and at temperature T_B which is in thermal contact with a reservoir at temperature T_{bath} via thermal conductance G_e is given in figure 2.2. The absorber is heated up by the incoming radiation. The temperature change is measured by the attached thermometer, exhibiting a temperature dependent resistance R(T). In microbolometer the resistance changing of the absorbing element in itself can be used as thermometer.

The values of heat capacity C and the thermal conductance G_e have influence on the bolometer performance, such as the voltage responsivity of the device to the absorbed radiation.

The bolometer temperature as a function of the time is the solution of the power balance equation(see eq. 2.1).

$$C\frac{dT_B}{dt} + G_e(T_B - T_{bath}) = P(t) \tag{2.1}$$

Assuming that the absorbed power changes periodically in time, $P(t)=P_0+\Delta P \cos(\omega t)$, the amplitude ΔT of the corresponding temperature modulation is given by:

$$\Delta T(\omega) = \frac{\Delta P(\omega)}{G_e + \sqrt{(1+\omega^2(C/G_e)^2)}} \tag{2.2}$$

The ratio $\tau \equiv C/G_e$ is the bolometer response time and it determines how fast the bolometer responds to a change in the absorbed power.

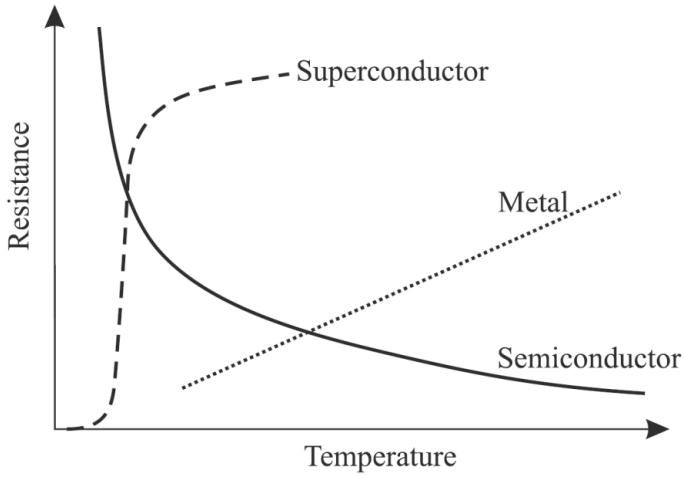

Fig. 2.1: Temperature dependence of resistance of three bolometer material types [48].

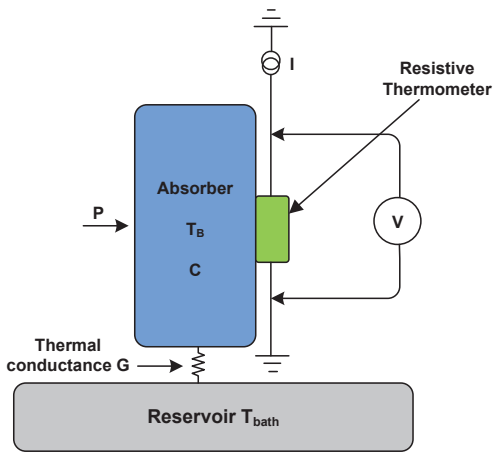

Fig. 2.2: Schematic of a bolometer thermally coupled to a reservoir.

Fig. 2.3: Schematic of a direct detector.

2.2 Bolometric detector

A bolometer can detect radiation in two different ways: direct detection (incoherent detection) and heterodyne detection (coherent detection). In direct detection mode, the received power is detected over a wide frequency range, whereas in heterodyne detection mode the RF signal is mixed with a local oscillator (LO) and down converted to intermediate frequency (IF) in the microwave range.

2.2.1 Direct detection

Figure 2.3 is a schematics of a direct detector. The bolometer responds to the power of the radiation. The RF signal (f_s) is amplitude modulated and the output voltage is measured using a lock-in amplifier or a voltmeter or a low noise amplifier etc. Since direct detector have a flat spectral response, frequency selection can only be obtained if a filter is placed in front of the detector. Important figures of merit that characterize the performance of the bolometer as direct detector are: the responsivity (S_V), the response time (τ) and the noise equivalent power (NEP) .

If the bolometer is biased at constant current I, the voltage responsivity is defined as the ratio between the voltage swing to the absorbed RF power.

$$S_V = \frac{\Delta V}{\Delta P} \tag{2.3}$$

In order to understand which parameters influence the responsivity of the bolometer a more careful analysis of the equation 2.1 has to be done. The bolometer absorbs a radiant power which usually has a steady part P_0 and a time varying part of amplitude P_1 and frequency ω (see eq.2.4).

$$P_B = P(t) = P_0 + P_1 e^{i\omega t} \tag{2.4}$$

The temperature of the bolometer consequently varies as:

$$T_B = T(t) = T_0 + T_1 e^{i\omega t} \tag{2.5}$$

The bolometer which is biased at constant current I, produces time varying electrical heat (DC heating) which can be written as:

$$I^2R(T) = I^2\left[R(T_0) + \left(\frac{dR}{dT}\right)T_1e^{i\omega t}\right] \tag{2.6}$$

The bolometer loses power $\overline{G}(\mathrm{T}_B\text{-}\mathrm{T}_{bath})$ to the reservoir through the thermal conductance G. It should be also noted that G in general is a function of the temperature [49] but it is here assumed to be constant for small temperature changes. Equating the input to the output power and taking into account the power stored in the heat capacitance, gives:

$$\begin{aligned} &P_0 + P_1e^{i\omega t} + I^2R(T_0) + I^2\left(\tfrac{dR}{dT}\right)T_1e^{i\omega t} = \\ &= \overline{G}(T_0 - T_{bath}) + GT_1e^{i\omega t} + i\omega CT_1e^{i\omega t} \end{aligned} \tag{2.7}$$

Where G is the dynamical thermal conductance dP/dT at the temperature T_0. Separating the time independent and the time dependent terms of the equation 2.7 yields to:

$$P_0 + I^2R(T_0) = \overline{G}(T_0 - T_{bath}) \tag{2.8}$$

$$\frac{\Delta P}{\Delta V} = P_1/T_1 = G + i\omega C - I^2(dR/dT) \tag{2.9}$$

The time independent terms gives the constant state heat flow equation that determines the operating temperature of the bolometer [49]. Using the equations 2.3 and 2.9 the voltage responsivity can be defined as:

$$S_V = \frac{\Delta V}{\Delta P} = I(dR/dT)T_1/P_1 = \frac{I(dR/dT)}{G - I^2(dR/dT) + i\omega C} \tag{2.10}$$

It is important to note that the responsivity is influenced by the electrothermal feedback i.e. when the resistance of the bolometer changes due to the absorbed power, the dc dissipation also changes. The result is the effective thermal conductance defines as:

$$G_e = G - I^2(dR/dT) \tag{2.11}$$

In order to characterize the bolometer (thermometer) is useful to introduce the temperature coefficient of resistance (TCR), α given by:

$$\alpha = \frac{1}{R}\frac{dR}{dT} \tag{2.12}$$

Plugging in equation 2.12 in equation 2.11 the effective thermal conductance can be written as:

$$G_e = G - I^2R\alpha \tag{2.13}$$

The corresponding time constant is τ=C/G_e. Plugging in the equation 2.13 in 2.10 the absorbed power responsivity can be written as:

$$S_V = \frac{IR\alpha}{G_e(1 + i\omega\tau)} \tag{2.14}$$

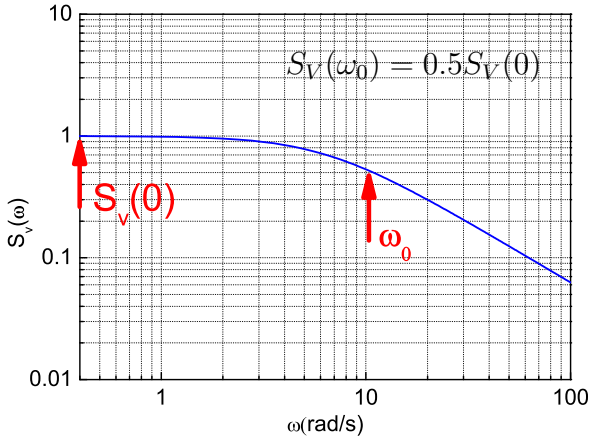

Fig. 2.4: Representation of the responsivity versus frequency

At an arbitrary modulation frequency ω the responsivity is defined as [49]:

$$S_V(\omega) = \frac{S_V(0)}{\sqrt{1+\omega^2\tau^2}} \tag{2.15}$$

Where $S_V(0)$=IRα/G_e is the responsivity at $\omega(0)$ (see fig.2.4). Semiconducting bolometers have negative α and G_e>G whereas semiconducting bolometers have positive α and G_e<G. The combination of having α>0 and a current bias, makes it possible that the effective thermal conductance equals to zero at a given current, resulting in a very high voltage responsivity. If the bolometer is voltage biased the same effect occurs when α<0. The thermal feedback influences the response time τ of the bolometer. The response time τ in the equation 2.15 determines the speed of the bolometer and as was mentioned earlier it is given by the ratio between the heat capacity and the thermal conductance. In many applications, it is important to have large bandwidth and high responsivity. The latter can be reached by reducing G_e but on the other hand this will make the bolometer slower. In order to keep τ small the heat capacitance C must be reduced by for example using low C materials. There are a few methods that can be used to increase the responsivity keeping the response time constant. If the heat flow into the substrate is the dominant bolometer cooling path, then the thermal conductance G_e equals the ratio between the bolometer area and the boundary resistance R_{bd} (see eq.2.16).Therefore making submicrometer bolometers leads to an increase of the responsivity.

$$G_e = \frac{A}{R_{bd}} \tag{2.16}$$

Other ways to increase the responsivity could be done by forming air bridge bolometer (see fig. 2.5) instead of having the bolometer directly on a substrate or using materials with larger temperature coefficient of resistance α.

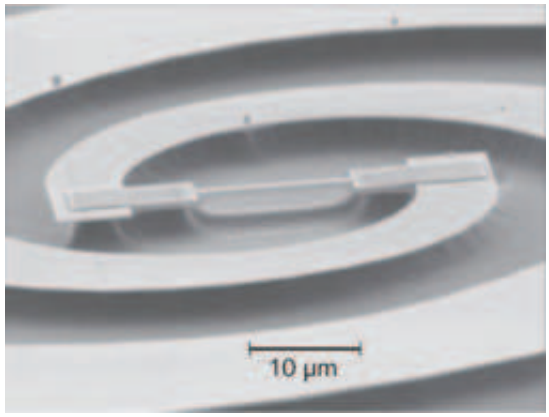

Fig. 2.5: Air bridge bolometer [50].

The sensitivity of a direct detector is quoted in terms of noise equivalent power (NEP). The NEP is defined as the radiant power that produces a signal to noise ratio of unity at the output of the receiver. The dominant noise contribution in a bolometer are the Johnson noise, the thermal fluctuation noise and the flicker noise. For 1 Hz bandwidth, the corresponding noise voltages are given below.

The Johnson noise is defined as [51]:

$$U_{J,n} = (4Rk_BT)^{0.5} \tag{2.17}$$

The thermal fluctuation noise which causes fluctuations of the temperature in the bolometer is given by [49]:

$$U_{FL,n} = (4k_BT^2G)^{0.5}S_V \tag{2.18}$$

At low frequency the flicker noise may become important. Because of its frequency dependence, the flicker noise is also called 1/f noise. The flicker noise is described by the following equation [49]:

$$U_{F,n} = i^x f(\omega) \tag{2.19}$$

where x depends on the device nature and f(ω) is the flicker noise frequency dependence. The overall noise equivalent power is calculated as [49]:

$$NEP^2 = \frac{4Rk_BT}{S_V^2} + 4k_BT^2G + \frac{i^{2x}f(\omega)^2}{S_V^2} \tag{2.20}$$

Table 2.1 shows some examples of cooled and uncooled bolometer performances.

2.2.2 Heterodyne mixing

Figure 2.6 is a schematic of down-conversion in a heterodyne receiver. The mixer is an electronic device (bolometer in this case) which has a non linear

Table 2.1: RESPONSIVITY (S_V), NOISE EQUIVALENT POWER (NEP) AND RESPONSE TIME (τ).

	S_V(V/W)	NEP(W/Hz$^{0.5}$)	$\tau(s)$
Air-bridge bolometer [50]	85	25x10^{-12}	0.2x10^{-12}
Monolithic Si bolometer [52]	2.4x10^{9}	10^{-17}	0.5x10^{-9}
Ti HEB [53]	-	3x10^{-19}	25x10^{-6}

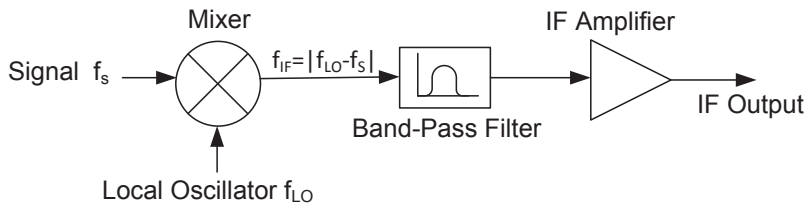

Fig. 2.6: Schematic of down-conversion in a heterodyne receiver. The mixer has two inputs ports for the local oscillator (LO) and the signal and one output port for the intermediate frequency (IF).

current-voltage (I-V) characteristic. The signal at the frequency (f_S) is mixed with local oscillator at frequency (f_{LO}) and down converted to an intermediate frequency f_{IF}. The voltage across the bolometer can be written as:

$$V(t) = V_{LO}\cos(\omega_{LO}t) + V_S\cos(\omega_S t) \tag{2.21}$$

where V_{LO} and V_S are amplitudes of the voltages of the local oscillator and of the signal at the input of the mixer. The power dissipated in the bolometer with a resistance R is:

$$P(t) = \frac{V^2(t)}{2R} \tag{2.22}$$

Inserting equation 2.21 in 2.22 and considering the average of the absorbed local oscillator and signal power (P_{LO}=V_{LO}^2/2R, P_S=V_S^2/2R) results in:

$$\begin{aligned} P(t) \;=\; & P_{LO} + P_S + P_{LO}\cos(2\omega_{LO}t) + P_S\cos(2\omega_S t) + \\ & +2\sqrt{P_{LO}P_S}\cos((\omega_{LO}+\omega_S)t) + \\ & +2\sqrt{P_{LO}P_S}\cos((\omega_{LO}-\omega_S)t) \end{aligned} \tag{2.23}$$

The bolometer cannot follow the power oscillation at $2\omega_{LO}$, $2\omega_S$ and $\omega_{LO}+\omega_S$ frequencies. These frequencies are higher than the IF bandwidth of the bolometer therefore they can be neglected in the equation 2.23. Defining $\omega_{IF} = \omega_{LO} - \omega_S$ the total radiation power, dissipated in the bolometer, can be written as:

$$P(t) = P_{LO} + 2\sqrt{P_{LO}P_S}\cos(\omega_{IF}t) \tag{2.24}$$

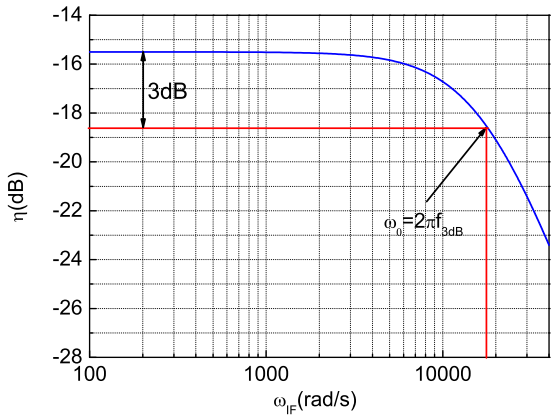

Fig. 2.7: Representation of the conversion gain as a function of the IF frequency

.

If the signal frequency is lower than the LO frequency the mixer operates in lower sideband (LSB) otherwise in upper sideband (USB). Systems which are sensitive to both sites are called double sideband (DSB). If the mixer operates in single sideband (SSB) only the upper sideband (USB) or the lower sideband is transmitted. More sophisticated approaches are realised in sideband separating (2SB) mixers where the USB and the LSB are separated at IF.

Important figures of merit which characterise a mixer are: the conversion efficiency or gain, the gain bandwidth and the mixer noise temperature. The conversion efficiency is defined as the ratio between the output power P_{IF} at IF frequency and the available signal power P_S at the input [36].

$$\eta_m(\omega_{IF}) = \frac{P_{IF}}{P_S} = \frac{2I^2C_0^2P_{LO}R_L}{(R_L+R_0)^2} \times \times \left(1 - I^2C_0\frac{R_L-R_0}{R_L+R_0}\right)^{-2} \times (1+\omega_{IF}^2\tau^2)^{-1} \quad (2.25)$$

Where C_0=dR/dT×1/G is the self heating parameter, R_L is the IF load impedance and R_0=V_0/I_0 is the bolometer DC resistance. The gain bandwidth (f_{3dB}) is defined as the IF frequency in which the conversion efficiency drops by a factor of two from the mixer gain at zero IF frequency (see fig. 2.7).

The mixer gain bandwidth is expressed by the following equation and it determine the mixer response time, τ_θ modified by the electrothermal feedback.

$$f_g = \frac{1}{2\pi\tau} \quad (2.26)$$

$$\tau = \frac{\tau_\theta}{1 - C_0\frac{R_L-R_0}{R_L+R_0}} \quad (2.27)$$

τ is the electron temperature relaxation time and τ_θ is the relaxation time for I_0=0. Figure 2.8 shows a schematic representation of a mixer.

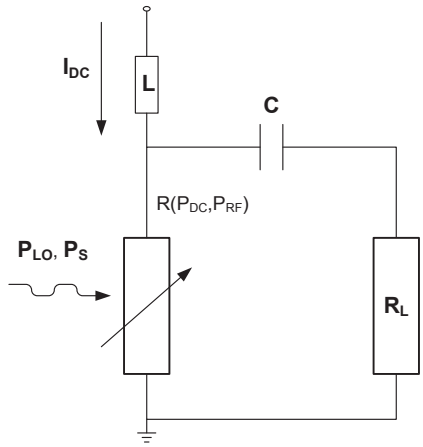

Fig. 2.8: Equivalent circuit of a bolometer mixer coupled to the DC and IF circuit.

The bolometer is biased in its resistive state by a DC current and by the RF radiation (LO power). In this situation no current flows through the IF load (R_L), because of the presence of the capacitor. Heterodyne conversion takes place when the LO is combined with a small signal (P_s), resulting in a modulation of the dissipated RF power in the mixer at the intermediate frequency. This generates an IF current in the circuit and leads to dissipation in the IF load. If the bolometer is biased at constant current, a small increase of the resistance leads to an increase of the DC dissipated power. The increase in the DC heating results in a further increase of the resistance and the results is a positive feedback. Positive feedback slows down the thermal response and destabilize the system. Negative feedback occurs when the bolometer is voltage biased. An increase in resistance causes a decrease of the DC dissipation and thus stabilizes the system and decreases the time constant. The electrothermal feedback is very important since affects the mixer performances.

The sensitivity in a mixer is quoted in terms of single sideband (SSB) or double sideband noise (DSB) temperature. The DSB noise temperature is more often quoted. The dominating noise sources in bolometer mixer are the thermal fluctuation noise and the Johnson noise [54]. Figure 2.9 is a representation of the receiver noise contributions. The output thermal fluctuation noise temperature due to the fluctuations in the electron temperature, T_e is given by [55]:

$$T_{FLn,out}(\omega_{IF}) = I^2 C_0 \frac{dR}{dT_e} T_e^2 \frac{4R_L}{(R_0+R_L)^2} \left(1 - I^2 C_0 \frac{R_L - R_0}{R_L + R_0}\right)^{-2} (1+\omega_{IF}^2 \tau^2)^{-1} \tag{2.28}$$

The Johnson noise, $T_{Jn,out}$ is equal to the noise in an ordinary resistor at temperature, T_e delivered in a load R_L(see eq. 2.29).

$$T_{Jn,out} = T_e \frac{4R_0 R_L}{(R_0+R_L)^2} \left(1 - I^2 C_0 \frac{R_L - R_0}{R_L + R_0}\right)^{-2} \tag{2.29}$$

The receiver output noise temperature is the sum of the the thermal fluctuation

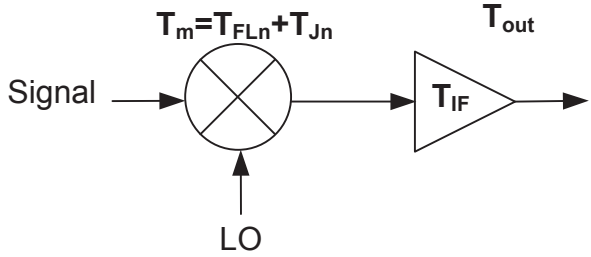

Fig. 2.9: Simplified picture of a receiver with noise contribution.

noise, Johnson noise and IF amplifier input noise.

$$T_{out}(\omega_{IF}) = T_{FLn,out}(\omega_{IF}) + T_{Jn,out} + T_{IF} \tag{2.30}$$

The DSB receiver noise temperature, referred to the receiver input is given by:

$$T_{rec}(\omega_{IF}) = \frac{T_{out}(\omega_{IF})}{\eta_m(\omega_{IF})} \tag{2.31}$$

Since the gain and the thermal fluctuation noise dependence on the IF have a single pole Lorentzian shape, the receiver noise temperature as a function of the IF frequency becomes:

$$T_{rec}(\omega_{IF}) = T_{rec}(0) + \frac{(T_{Jn,out} + T_{IF})}{\eta_m(0)}(\omega_{IF}^2\tau^2) \tag{2.32}$$

Figure 2.10 shows a theoretical plot of the noise contributions in a receiver. The noise bandwidth can be expressed by the equation 2.33 and it is defined as an IF where T_{rec} rises by a factor of two.

$$f_n \approx f_g\sqrt{\frac{T_{FLn,out} + T_{Jn,out} + T_{IF}}{T_{Jn,out} + T_{IF}}} \tag{2.33}$$

The noise bandwidth is larger than the gain bandwidth [56]. This is due to the fact that the main contribution to the noise is the thermal fluctuation noise T_{FLn}. In fact the Johnson noise T_{Jn} is flat at the output of the mixer, while the thermal fluctuation noise starts to rolls off at the same frequency of the conversion gain [56].

Due to the long response time bolometers are not practical for mixing. In the submillimeter range receivers with large bandwidth are needed, in fact they should be fast enough to follow the IF frequency which is a replica of the original RF spectrum [57]. A large IF bandwidth is important in the measurement of broad emission lines from external galaxies as well as simultaneous observation of several molecular lines. The technology that can meet this requirement are hot electron bolometers (HEB) based on superconductors films.

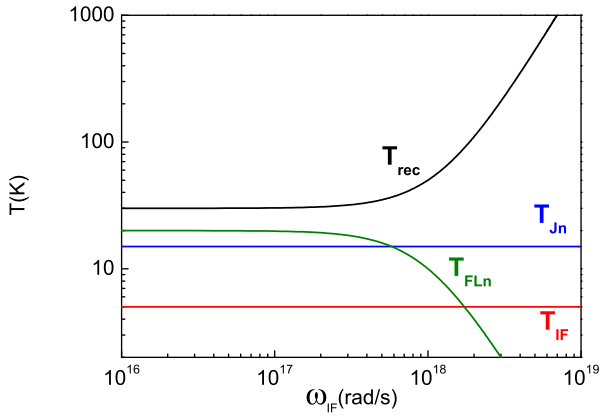

Fig. 2.10: Theoretical plot of the noise contributions in a receiver

.

2.3 Hot electron bolometer mixers

Hot electron bolometer mixers using semiconductors were invented in the early 1970s [58], however the development of superconducting versions of this basic concept has lead to the most sensitive mixers at frequencies in the terahertz region. Hot electron bolometer mixers are a thin superconducting strip on a dielectric substrate coupled between contact pads (see fig.2.11). Compared to a resistive bolometer, in which the whole bolometer is heated up after it absorbs radiation, in the HEB only free electrons are heated up. Superconducting HEBs can be integrated with any planar antenna (i.e. logarithmic spiral or twin-slot antenna) as well as with waveguide [59]. HEB, operating as a mixer, is cooled down below its critical temperature. At low temperature ($T<T_c$), the thermal coupling between free electrons and phonons in the superconducting bridge is weak while the electron-electron interaction is strong. If a radiation (LO power) is coupled in the HEB, the electron-electron interaction is broken and free electrons diffuse in the contact pads or they interact with phonons in the microbridge and escape into the substrate. There are two types of cooling mechanisms which determine the electron relaxation time and consequently the gain bandwidth of an HEB mixer. These mechanisms are the diffusing and phonon cooling. If the length of the microbridge is shorter than of the thermal diffusion length $L_{th}=(D\tau_e)^{1/2}$ of the superconducting material, the cooling mechanism occurs by outdiffusion of the electrons in the contact pads within a time, $\tau_{diff}=(L^2/\pi^2 D)$. HEB mixers based on this principle are called diffused-cooled [42]. If the length of the microbridge, L is larger of the thermal diffusion length, L_{th} cooling by phonons dominates. These mixers are called phonon-cooled.

Figure 2.11 shows a picture of an HEB with a representation of the phonon and diffusion cooling mechanism. In phonon-cooled HEB [28] the crucial parameter is the interface between the superconducting film and the substrate whereas in diffusion cooling the crucial parameter is the interface between the

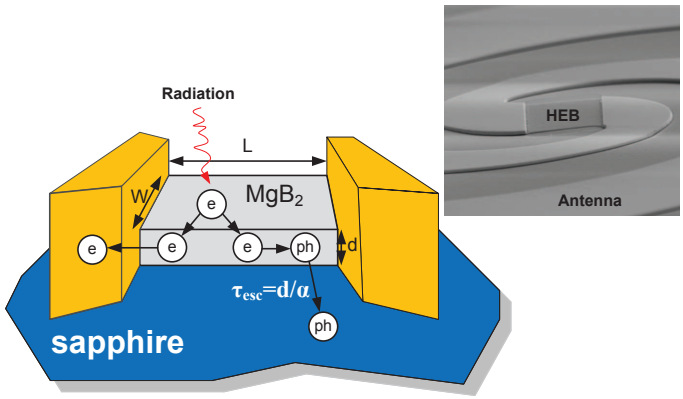

Fig. 2.11: Simplified picture of a superconducting Hot Electron Bolometer with phonon and diffusion cooling mechanism. The SEM image shows a phonon-cooled HEB integrated with spiral antenna.

film and the contact pads. In the low-temperature limit, when the electron specific heat, c_e is much larger than the phonon specific heat, c_{ph}, the electron temperature relaxation time is governed by a single time constant,τ_θ [60]. The total electron relaxation time which determines the speed of the bolometer is given by:

$$\tau_\theta = \tau_{e-ph} + \frac{c_e}{c_{ph}}\tau_{esc} \tag{2.34}$$

Where τ_{e-ph} is the electron-phonon interaction time which is a function of the temperature T [61]:

$$\tau_{e-ph} = T^{-\mu} \tag{2.35}$$

The value of μ has been reported between 2 and 4 for various materials [62]. τ_{esc} is the escape time of the phonons in the substrate which is dependent on the thickness of the film d, the speed of the sound u and the film/substarte acoustic phonon transmission coefficient β.

$$\tau_{esc} = \frac{4d}{\beta u} \tag{2.36}$$

The terms c_e and c_{ph} in the equation 2.34 are the electron and phonon specific heats which are also dependent of the temperature of the film.

In conclusion, to have a fast response of the phonon-cooled HEB mixer it is required to have thin films with higher critical temperature. On the other hand the critical temperature decreases with thinner film thickness, which mostly occurs due to the large number of defects of the first layer of the film. An optimum between these two parameters must be found to maximize the IF bandwidth.

2.4 Basics of superconductivity

This section concerns the basics of the superconductivity with focus on the important parameters of a superconductor.

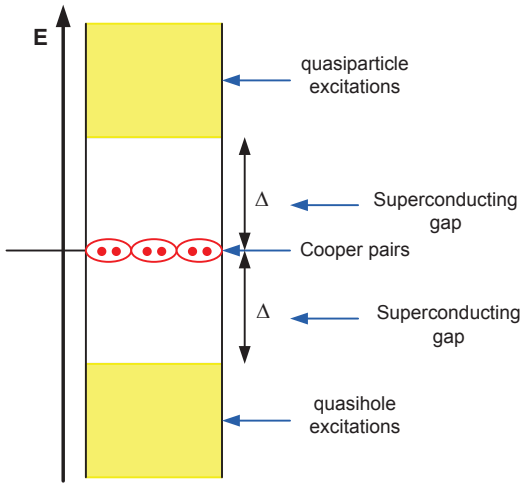

Fig. 2.12: Energy diagram of a superconductor

Two basic properties of a superconductor are: the perfect diamagnetism and the zero resistance to a dc current. At certain temperature called critical temperature, T_c, the resistance of a superconductor drops to zero and remains zero at all temperatures below T_c. Below T_c the conduction electrons form pairs, called Cooper pairs which can carry current (supercurrent) without any resistance. Cooper pairs are also responsible of the perfect diamagnetism of a superconductor known as the Meissner effect. Indeed at the temperature below T_c a magnetic field is expelled from the interior of a superconductor.

Superconductors can be divided in two classes: type-I and type-II. Type-I exhibits positive superconductor-normal interface energy while type-II negative interface energy [63]. Type-I is a perfect diamagnet. In fact below a critical magnetic field, H_c, there is no penetration of the flux in the superconductor but above the critical field the material is driven in the normal state and the the flux starts to penetrate. Type-II has more complex magnetic properties. There are two critical fields for such type of superconductor, H_{c1} and H_{c2}. If the magnetic field applied is below H_{c1}, the superconductor expels the magnetic flux while if the magnetic field is in the range $H_{c1}<H<H_{c2}$ some magnetic fluxes are trapped in the material. At $H>H_{c2}$ the material becomes normal.

The energy gap Δ, the London penetration depth λ_L and the coherence length ξ, together with the critical temperature and the critical magnetic fields are very important parameters which characterize a superconductor.

The energy gap Δ is related to the critical current [63] through the equation 2.37 . It separates the energy level of ground state (Cooper pairs level) and the energy levels of the quasiparticle excitations (see fig.2.12).

$$\Delta(0) = 1.74 k_B T_c \tag{2.37}$$

The minimum energy to break the Cooper pairs and create two quasiparticles is

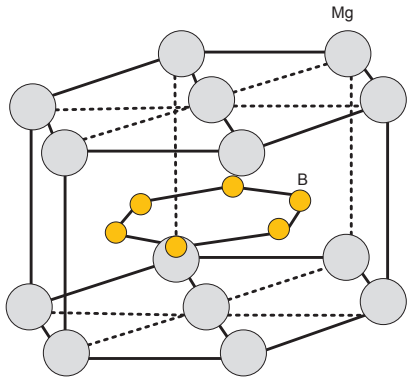

Fig. 2.13: MgB_2 crystal structure. The magnesium atoms show an hexagonal layer, while the boron atoms a graphite like honeycomb layer [43] .

2Δ. The penetration depth, λ_L, in a superconductor refers to the exponentially decaying of the magnetic field at the surface of the superconductor. It is the distance required to fall to 1/e times the externally applied magnetic field [63].

$$\lambda_L = \left(\frac{\varepsilon_0 m c^2}{n e^2} \right)^{1/2} \tag{2.38}$$

Where n is the superconducting electron density. The coherence length, ξ, is related to the Fermi velocity and the energy gap of the superconducting material.

$$\xi = \frac{\hbar v_F}{2\Delta} \tag{2.39}$$

The ratio between the penetration depth and the coherence length is an important parameter which determine if the superconductor is type-I or type-II.

$$k = \frac{\lambda_L}{\xi} \tag{2.40}$$

More precisely, $0 < k < 1/\sqrt{2}$ gives a type-I superconductor whereas if $k > \sqrt{2}$ gives a type-II superconductor [63].

2.4.1 Magnesium diboride films MgB_2

The superconductivity in magnesium diboride MgB_2 was discovered by Akimitsu´s group in 2001 [43] and since then great interest has been generated in the research field. MgB_2 is a conventional intermetallic compound superconductor (not based cooper-oxide superconductor) with the highest critical temperature (39 K in the bulk) that as been reported so far. Before the discovery of MgB_2 the highest superconducting transition temperature was reported for Nb_3Ge (23 K) material [64]. The model of the crystal structure of the MgB_2 is shown in figure 2.13. The crystal consists of Mg planes containing just magnesium and B_2 plane containing just boron, which are layered alternatively along the c axis. X-ray diffraction spectrum indicates an hexagonal crystalline structure,

where the lattice constants are: a=0.3086 nm and c=0.3524 nm [65]. Study of the MgB_2 energy gap has shown that it is has two energy gaps, one at lower energy $\Delta(0) \sim 2$ meV and one at higher energy $\Delta(0) \sim 7$ meV [66]. The values of the energy gaps allow the conclusion that MgB_2 superconductor combines characteristics of both type-I and type-II superconductors.

When a superconductor material is chosen for the fabrication of phonon-cooled HEB mixers fundamental parameters must be taken into consideration such as the critical temperature and electron phonon interaction time. Indeed, it has been established that the IF gain bandwidth is correlated to these parameters as well as to the film thickness, film´s speed of the sound and acoustic match film/substrate. A low noise temperature and low LO power requirements determines the choice of HEB mixer for the Herschel space observatory. However, HEB mixers made on NbN film exhibit a limited gain bandwidth to only 3-4 GHz in very thin films (3-4 nm) [67]. Further reduction of the NbN film thickness leads to a drastic reduction of the critical temperature which weakens the electron-phonon interaction time. In order to increase the gain bandwidth of HEB mixers a solution is to search for material with faster response.The high critical temperature of MgB_2 film (39 K in the bulk), makes it very attractive to replace NbN with MgB_2, aiming for better performances. Recently it was demonstrated that even thin MgB_2 films (7.5 nm) can exhibit a critical temperature as high as 34 K [45]. Furthermore, using time domain spectroscopy, the electron-phonon interaction time as been measured to be 3 ps in a thin film MgB_2 in a silicon substrate [46] which is shorter compared to NbN film. Indeed in thin NbN films the electron-phonon interaction time has been measured to be 12 ps at 10 K [47] whereas the escape time was 40 ps [67]. Considering the higher critical temperature and shorter electron-phonon and phonon escape time of MgB_2 film compared to NbN film, HEB mixers based on MgB_2 have been investigated, characterized and fabricated.

Chapter 3

MgB_2 HEB fabrication process and DC characterisation

A number of devices with micrometer sizes has been fabricated using UV-lithography, ion milling and lift-off process. Lately, submicrometer devices have been fabricated using the electron beam lithography. The main challenge during the fabrication of the HEBs is to preserve the quality of the MgB_2 film (in the micro/nano bolometers) and to get a high yield with a reproducible processing. Indeed, it has been demonstrated that MgB_2 degrades when it is exposed to the water and oxygen [68, 69].

In this chapter a detailed description of the device fabrication process as well as the DC test results will be presented.

3.1 UV-Lithography process

Devices with different bolometer area have been fabricated. The area was in the range of 100-500 μm^2 and 3-42 μm^2. HEBs were fabricated on 30 nm, 15 nm and 10 nm thick MgB_2 films. MgB_2 films were grown on c-cut sapphire substrates via molecular-beam epitaxy (MBE). Mg and B were evaporated using e-guns and the growth temperature measured at the backside of the substrate holder was 300 °C [70, 71]. In order to prevent the film degradation during the devices fabrication as well as to improve the MgB_2/Au contact resistance, the films were covered by a 20 nm in situ gold layer.

The critical temperature, T_c was 25, 23 and 19 K as measured in the continuous 30, 15 and 10 nm films, respectively.

The fabrication of the MgB_2 HEBs consisted on several processing steps, as follows:

- **HEB length definition:** The first step is to define the bolometer length by using image reversal resist followed by the deposition of a Ti/Au (5 nm/350 nm) metal stack and subsequent lift-off. (see fig. 3.2 (b)).

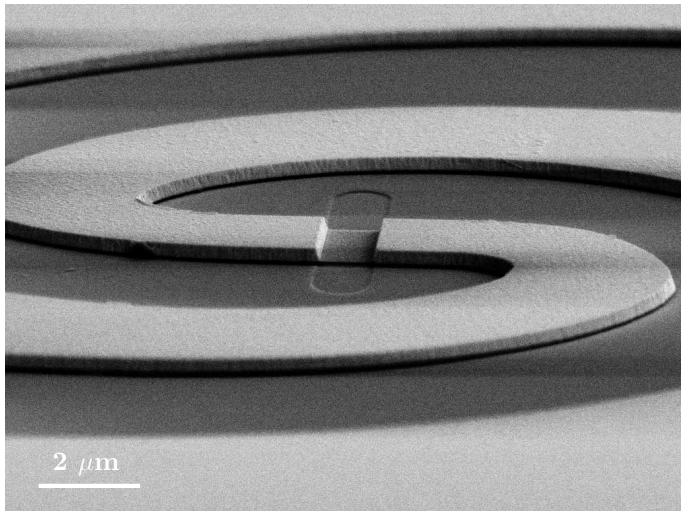

Fig. 3.1: SEM image of MgB_2 HEB integrated with spiral antenna (grey) on sapphire substrate (black)

- **Etching**: The $in-situ$ 20 nm thick gold layer over the bolometer bridge was etched via Argon ion milling. This step was quite critical, since a too short etch might leads to residues of gold over the bolometer, whereas a too long etch could etch the MgB_2 film (see fig.3.2 (c) and (d)).
- **Antenna and HEB width definition:** In this step the spiral antenna, in which the inner part corresponds to the bolometer width, and chip frames were defined using positive photoresist. The chip frames allowed to keep the bolometer short circuited once the antennas were fabricated (see fig.3.2 (e)).
- **Etching and final device:** The resist over the antenna and the chip frames was used as etching mask to protect the patterns during the etching. The thick gold layer as well as the MgB_2 film were etched down to the substrate via Argon ion milling (see fig.3.2 (e) and (f)).
- **Dicing**: In order to perform the DC and RF tests, the wafer was cut along the chip frame lines into chips of size 1.5×3.8mm.

Figure 3.1 shows a scanning electron microscope (SEM) image of an HEB bolometer integrated with spiral antenna completely made using the UV-lithography, lift-off and ion milling process. The fabrication process sequences are shown in 3.2. Several problems have been found during the fabrication of MgB_2 HEBs. In addition to the film degradation during processing steps, it was found that the use of a carbon mask (deposited using Pulsed laser deposition and lift-off process) for defining the antenna pattern and the HEB width leaded to a low yield. After fabrication the devices showed very high impedance. Focused ion beam SEM (FIB-SEM) and SEM analysis were performed in not working devices, revealing a physical disconnection between the bolometer and antenna pad. This is clearly visible in figure 3.3 and it was

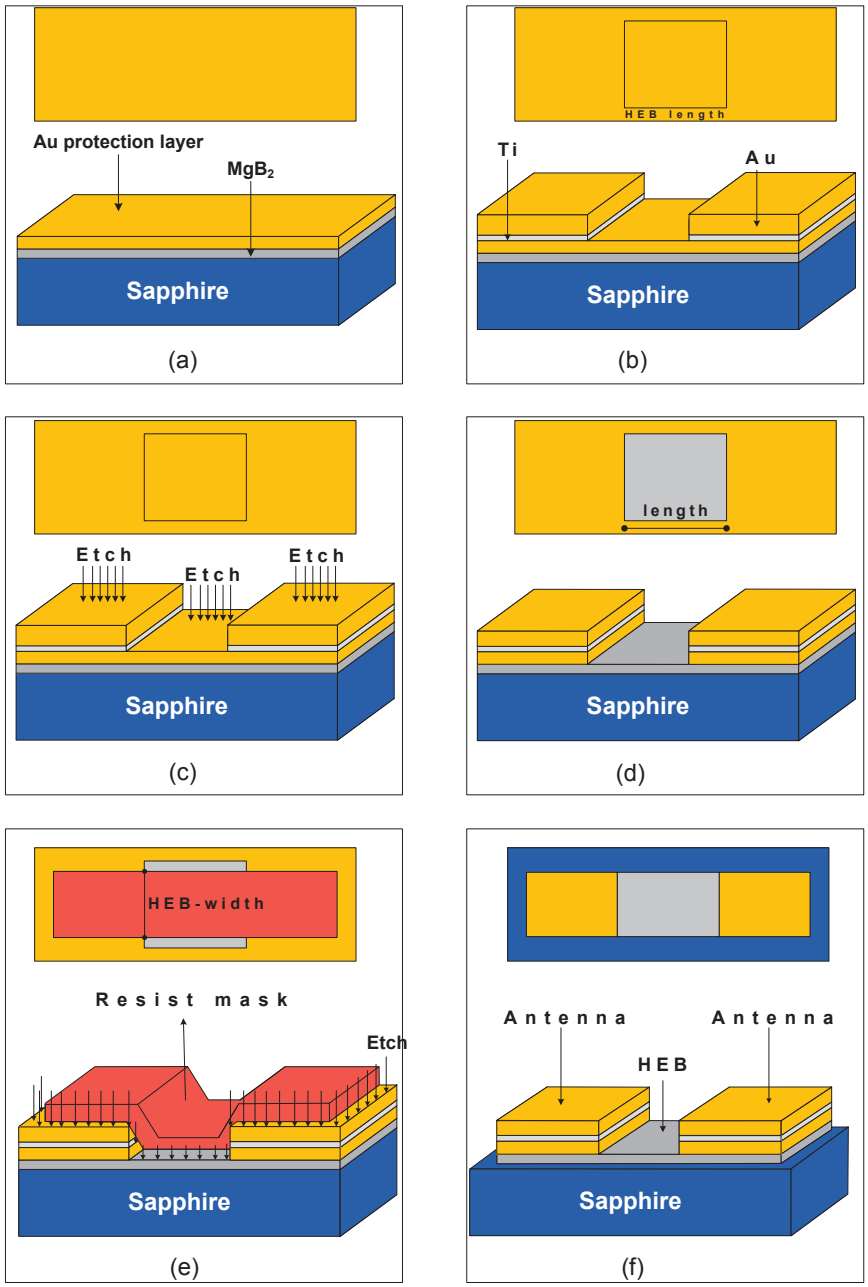

Fig. 3.2: Fabrication process sequences. (a) Wafer. (b) HEB length definition. (c-d) Etching of the thin layer of gold. (e) Antenna and HEB width definition. (e-f) Etching and final device.

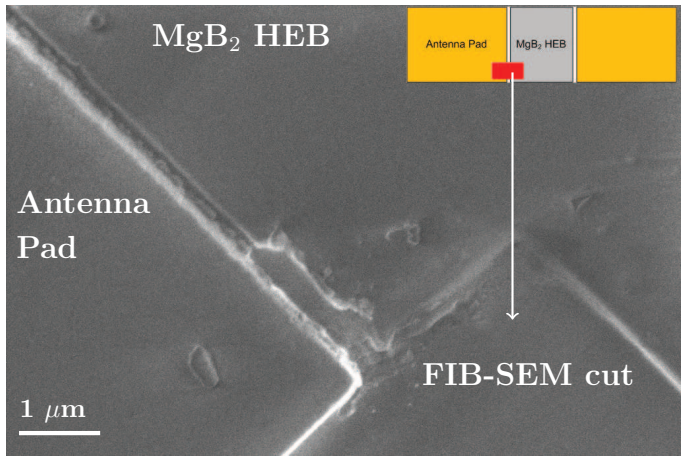

Fig. 3.3: SEM image of the HEB performed after the FIB-SEM analysis. The image clearly shows that the bolometer is disconnected from the antenna pad.

caused by the non uniformity in the carbon mask thickness along the wafer. However, these problems have been solved using a resist mask, indeed the processing was more reproducible.

3.2 Electron beam lithography process

In order to reduce the local oscillator power requirement and to push the HEB mixers towards higher frequencies, submicrometer devices have been fabricated employing electron beam lithography. The bolometer area was in the range of 0.09-0.64 μm^2. The fabrication of the bolometer was done by several electron beam lithography steps and lift off process as follows:

- **Alignment marks and chip frames**: First, the alignment marks and the chip frames were fabricated. The alignment marks are needed in order to align the patterns of subsequent processing steps. The chip frames allowed to keep the bolometers short circuited once the antennas were fabricated. This avoids possible electrostatic charge that can permanently damage the devices.. After the lithography, metals deposition (Ti/Au) and lift off were performed.

- **Contact pads**: The device fabrication starts with the lithography of contact pads which define the bolometer length. At this stage Ti (10nm), Au (100nm) and Ti (30nm) were deposited. The top Ti layer was used to protect the pads during ion milling (see 3.4(a)).

- **Antenna**: The antennas were patterned in this step and Ti (10nm), Au (250nm) and Ti(30nm) layers were used for the metallization of the antennas. The top layer of Ti was deposited for the same purpose in the previous processing step. The center part of the antenna has an overlap with the contact pads (see 3.4(b)).

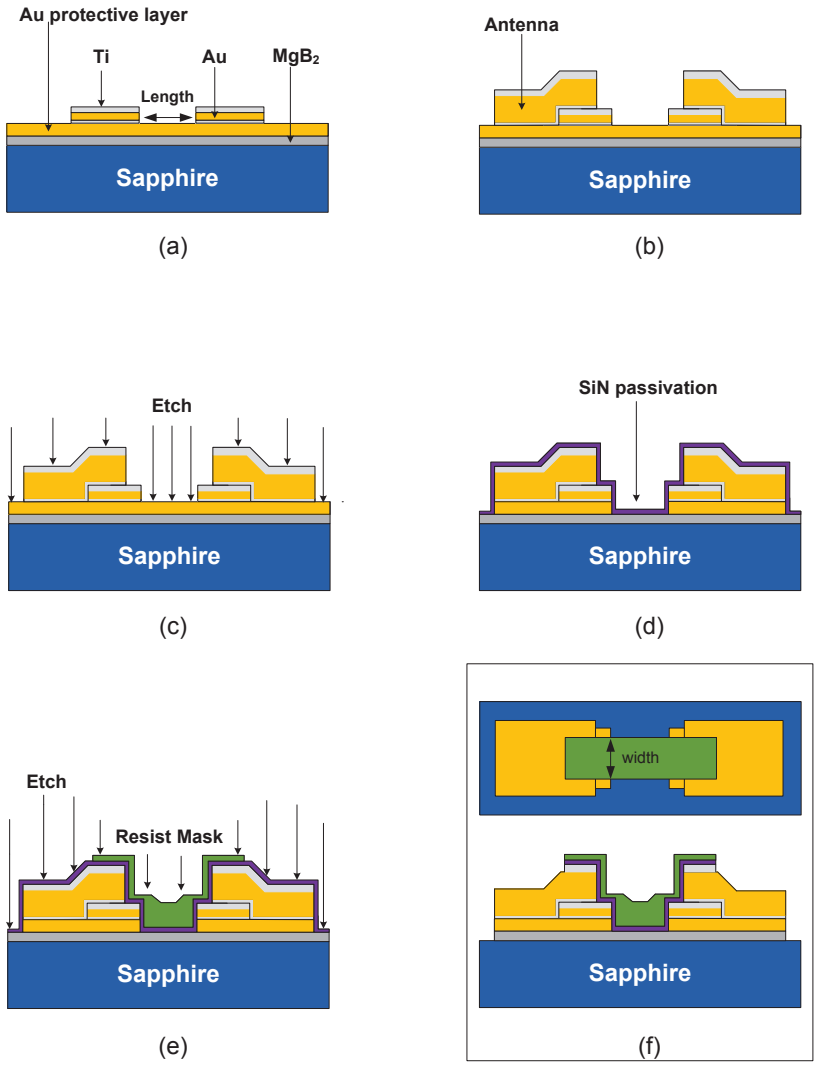

Fig. 3.4: Fabrication process sequences: (a) Contact pads. (b) Antenna. (c-d) Etching of the thin layer of gold and passivation. (e) Bolometer mask and etching. (f) Final device.

- **Etching and passivation**: At this stage the 20 nm thick $in-situ$ Au layer was etched away using Argon ion milling. To prevent the degradation of the MgB_2 film during the rest of the processing steps, immediately after the etching, the devices were passivated by 40 nm thick SiN_x film. The SiN_x film was deposited $ex-situ$ using RF magnetron sputtering see (see 3.4(c-d)).

- **Bolometer mask and etching**: Negative e-beam resist was used as etching mask in order to define the bolometer width. Subsequently, the SiN_x passivation and MgB_2 film were etched in the regions not protected by the resist. (see 3.4(e-f)).

Finally, a diamond saw was used to cut the wafer along the chip frame lines into chips of size 1.5×3.8mm. The fabrication process sequences are shown in 3.4.

3.3 DC characterisation

In this section the DC results are presented and discussed. Before starting the RF characterization, DC tests were performed in the fabricated devices. In order to measure the resistance versus temperature curve, the devices were biased at constant current (typically $1\mu A$) and the voltage was measured while the devices were cooled from room temperature (300 K) to 4.2 K. At the temperature of 4.2 K, current versus voltage curve was recorded by swiping the voltage until the current exceeded the critical current, I_c. At this point the photons absorbed in the superconducting bridge brake the Cooper pairs and creates quasiparticles and the devices are driven in the normal state. Figure 3.5

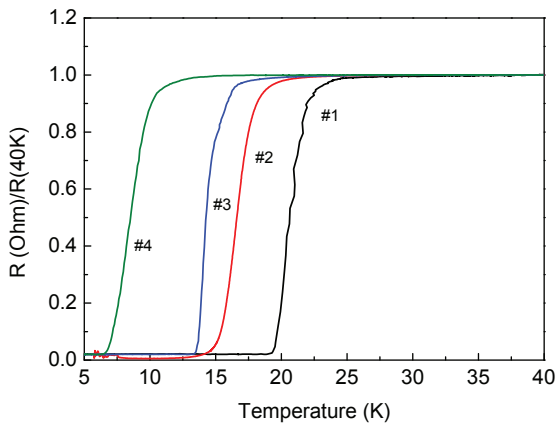

Fig. 3.5: Resistance versus temperatures curves of HEBs. Sample numbers correspond to table 3.1. The curves are normalized to the reistance at 40 K.

shows resistance versus temperature curves of HEBs patterned in MgB_2 films with different thicknesses (30nm, 15nm and 10nm). The critical temperature

Table 3.1: MgB_2 THICKNESS (d), CRITICAL TEMPERATURE (T_c), TRANSITION WIDTH (ΔT_c), RESISTIVITY (ρ_{300}) AND RESISTANCE AT 300 K (R_{300})

Device	Batch	d(nm)	Δ T_c(K)	T_c(K)	R_{300} (Ω)	$\rho_{300}(\mu\Omega \times cm)$
1	A	30	1	22	45	90
2	B	15	2	17	180	105
3	C	10	1.5	15	130	165
4	D	10	2	8.5	86	190
5	C	10	1.5	15	190	221

decreases with the thickness, which mostly occurs due to the larger number of defects in the first layers of the film. Devices of batches C and D are made of 10 nm films. However, due to the differences in the initial quality of the films, the T_c of this two batches is 15K and 8.5K respectively. A summary of the figure 3.5 is also presented in table 3.1. The MgB_2 room temperature resistivity after the fabrication ranged from $90\mu\Omega \times cm$ (30nm film) to $220\mu\Omega \times cm$ (10nm film). The sheet resistance ratio, R(300)/R(40), was approximately 1.3, which together with the high resistivity indicates that the MgB_2 films are in the dirty limit [72].

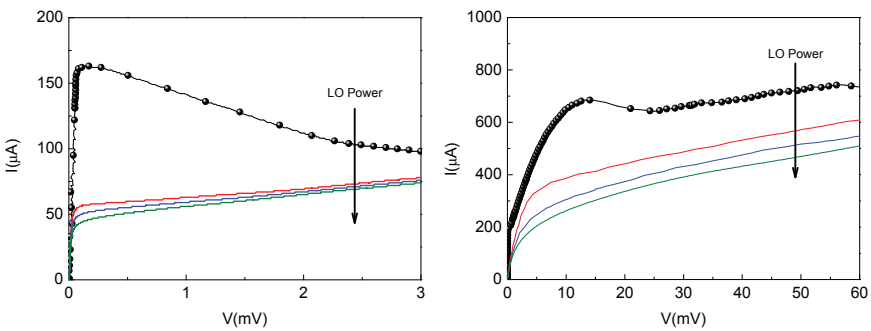

Fig. 3.6: (a) I-V curves of 1 μm × 3 μm, device #4. (b) I-V curves of 6 μm × 7 μm, device #5. HEBs at 4.2 K bath temperature, with LO power and without LO power applied.

I-V characteristics of MgB_2 HEBs #4 and #5 (of 1 μm × 3 μm and 6 μm × 7 μm, respectively), with and without local oscillator (LO) power applied, are shown in figure 3.6. The room temperature resistance of these devices were $R_{\#4}$(300K)=86Ω and $R_{\#5}$(300K)=190Ω whereas the resistivity of the bridges were $\rho_{\#4}$(300K)=$190\mu\Omega \times cm$ and $\rho_{\#5}$(300K)=$221\mu\Omega \times cm$. The critical currents, measured at 4.2 K, were 160μA and 650μA for samples #4 and #5, respectively. The resulting critical current densities were 0.55 MA/cm^2 and 0.93 MA/cm^2. Upon application of the LO power the critical current in the HEBs is suppressed. Due to the lower T_c and the smaller bolometer size, the required LO power for device #4 was much smaller compared to device #5.

The receiver noise temperature T_{rec} was measured for devices #4 and #5, whereas for other devices T_{rec} was not measured because of the lack of the LO power. Results about IF bandwidth will be presented in the next section.

The DC results that have been presented in these section are about HEBs that have been fabricated with photolithography process. However devices made using ebeam lithography have been successfully fabricated and they are under tests.

As said above, before starting RF measurements in the fabricated devices, it is important to perform DC tests in order to understand the quality of the devices.

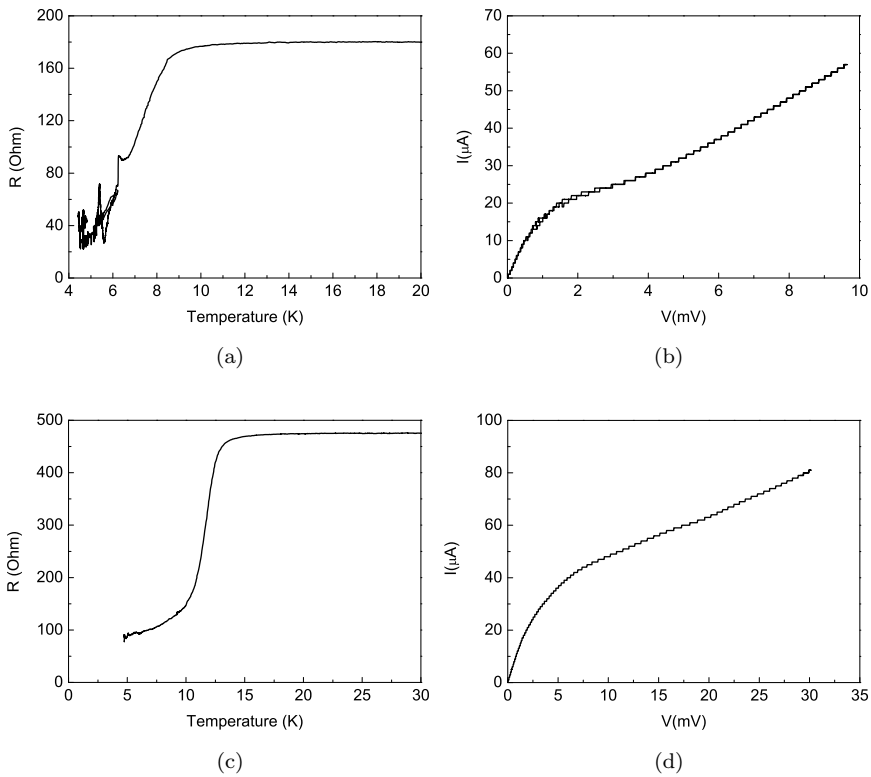

Fig. 3.7: Examples of Resistance versus temperature (R-T) and current versus voltage curves (I-V) for poor devices.

Figure 3.7 shows some examples of R-T and I-V characteristics of devices fabricated in 10 nm MgB_2 film with poor performances. Important parameters that must be analyzed during the DC tests are: the critical temperature (T_c), the transition width (ΔT_c) and the residual resistance. Usually, the RF measurements are performed near the critical temperature since at this point (in good samples) the maximum sensitivity can be achieved in the device under test. Sharp transition between the normal state and superconducting state (ΔT_c very small) is needed to get high sensitivity. As discussed in chapter 2 it is important to have high T_c of the superconducting bridge since the latter

is directly correlated with the speed of the device and consequently with the gain bandwidth. High T_c is desiderate to get wider gain bandwidth. The residual resistance which is the resistance at the bath temperature (4.2 K in this case) must be zero or very close to zero to have a good quality of the superconducting material. As is possible to see from the DC measurements of figure 3.7, these devices were not suitable for doing RF tests. Indeed they did not reach the superconducting state, the T_c was very low for one of them and finally they had broadband transition.

Chapter 4

THz characterisation and discussion

In order to characterise the MgB_2 mixers performance, the mixer gain and the noise temperature measurements were performed across a wide IF band, at various bias conditions and LO power levels. In this chapter the experimental data are presented as well as analyzed using the two-temperature model.

4.1 Experimental technique

For the RF measurements the MgB_2 mixer chips ($\#1-5$ see section 3.3) were glued on the backside of a 12 mm elliptical silicon lens, without an AR-coating, defining a quasi-optical setup. The mixer block was placed on the cold plate of a LHe cryostat (4.2 K bath temperature). Figure 4.1 shows the setup used for the gain bandwidth measurements. The gain bandwidth of the devices $\#1-3$ was measured using two backward wave oscillators (BWOs) at 600 GHz. The frequency of the Local oscillator (LO) BWO was kept constant, while the frequency of the signal BWO was tuned. At each frequency point, the amplitude of the signal was modulated by a mechanical chopper at 18 Hz. The direct

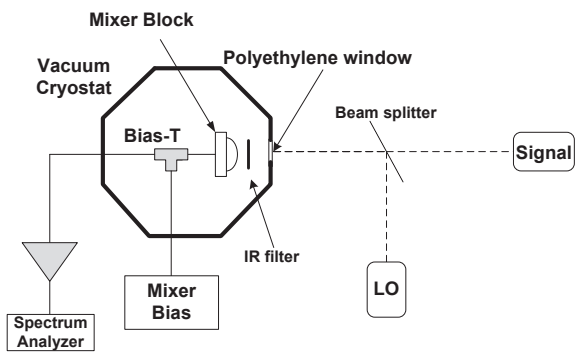

Fig. 4.1: The gain bandwidth measurement setup

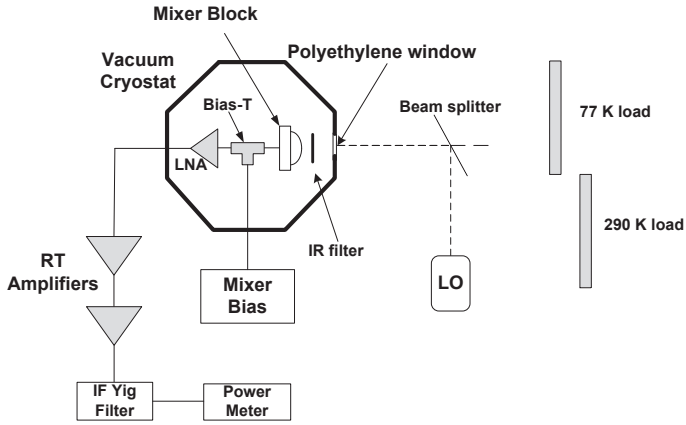

Fig. 4.2: The noise temperature measurement setup

detection signal was read out via the mixer bias line with a lock-in amplifier, which was later used for the calibration of the signal input power. The IF signal was amplified and measured by a microwave spectrum analyzer. Both the LO and the signal beams were collimated by Teflon lenses, spatially mixed by a thin film (Mylar^{TM}) beam splitter, and led into the cryostat through a high density polyethylene pressure window. Three sheets of Zitex G108 IR filters were installed at the 77 K and 4.2 K shields.

The optimal LO power for HEB mixers scales with the critical temperature and the bolometer size [60]. Furthermore, efficient coupling of the LO power to the HEB mixer occurs only when the photon energy is larger than the energy gap of the MgB_2 film 2Δ. Therefore, for a mixing experiment at 600 GHz, devices $\#1-3$ were heated to a temperature a few Kelvin below T_c.

The noise temperature for devices #4 and #5 was measured using the Y-factor technique with a 290 K and a 77 K (liquid nitrogen) black body sources (Eccosorb sheets [73]). The 600 GHz BWO local oscillator was used, as in the previous measurements. The intermediate frequency signal from the mixer was amplified using a set of cold and room temperature low noise amplifiers. Cold low noise IF amplifiers covered frequency ranges of 1-4 GHz and 4-8 GHz. The IF passband was set by a tunable (1-9 GHz) 50 MHz band pass filter (see fig. 4.2).

The gain of the device #4 was extrapolated from the Y-factor measurements using an expression P_{if}=(P_{300}-P_{77})×G_m, where P_{300} and P_{77} are the single mode Planck power in the IF bandwidth, and G_m is the mixer gain. The measured data were fitted with a single-pole Lorentzian 4.1 where G(0) (the mixer gain at zero IF frequency) and f_g (the 3 dB gain roll-off frequency) were used as fitting parameters.

$$G(f_{IF}) = G(0)[1 + (f_{IF}/f_g)^2]^{-1} \tag{4.1}$$

The effective mixer time, τ constant is obtained as τ=$1/(2\pi\ f_g)$. The gain bandwidth depends on the HEB mixer bias point because the electrothermal feedback modifies the mixer time constant as $\tau = \tau_\theta/(1 - C_0(R_L - R_0)/(R_L +$

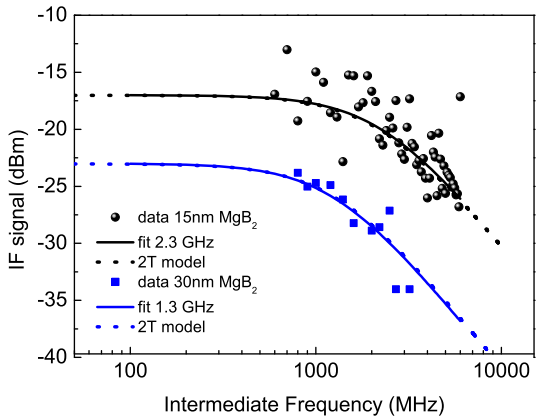

Fig. 4.3: Intermediate frequency response of MgB_2 mixers made of 15 nm (top curves) and 30 nm (lower curves) MgB_2 films. Solid lines are fits to the experimental data. Dashed lines are results of the two-temperature model.

$R_0)$), where τ_θ is the time constant in the limit of a zero bias, C_0 =(R_d-R_0)/(R_d+R_0) is the self heating parameter, R_0=V/I is the dc resistance at the mixer bias point, R_d is the differential resistance (dV/dI) and R_L is the IF load resistance (50 Ω) [74].

4.2 Results

In chapter 2 it has been established that the IF gain bandwidth of phonon-cooled HEB mixers depends on several parameters such as the film thickness d and the critical temperature T_c. HEB mixers with the MgB_2 film ranging from 30 nm to 10 nm have been investigated. The relative mixer gain as a function of the intermediate frequency of the mixers fabricated from 30 nm(lower curves) and 15 nm(upper curves) MgB_2 films is given in 4.3. Figure 4.4 shows the response of HEBs fabricated from 10 nm films. The GBW was obtained by fitting the measured data with the equation 4.1. The 3 dB gain roll-off frequency was 1.3 GHz and 2.3 GHz for devices 1 and 2 fabricated from 30 nm and 15 nm films. A GBW of 3.4 GHz was observed for the mixer #3 made of a 10 nm film with a T_c of 15 K. Much smaller GBW, 1.5 GHz, was measured for a mixer #4 fabricated from the films with the same thickness (10 nm) but with a T_c of 8.5 K. The corresponding mixer time constant τ is given in Table 4.1.

These results clearly show the dependence of the gain bandwidth with the thickness and critical temperature of the film. In figure 4.5, the GBW data to the film thickness and the critical temperature for both MgB_2 mixers (this work) and NbN mixers (from the literature) are correlated. The open symbol in figure 4.5(a) correspond to the MgB_2 sample #4. The solid lines in the figure 4.5(a) are the fit to the experimental data. In order to estimate the GBW for thinner MgB_2 films, the fit for the GBW as a function of the thickness has been

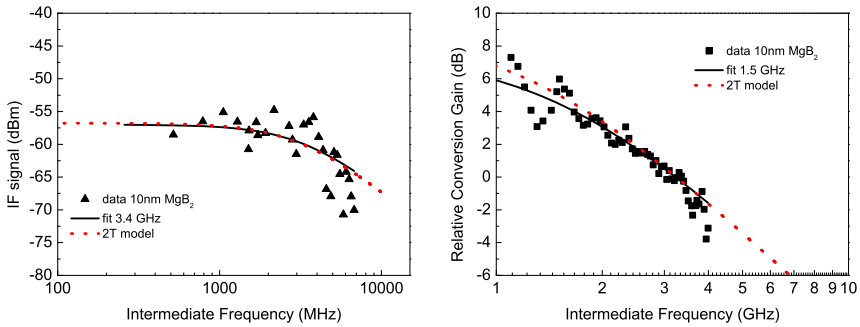

(a) (b)

Fig. 4.4: (a) Intermediate frequency response of MgB_2 mixers made of 10nm (batch C) film. (b) IIntermediate frequency response of MgB_2 mixers made on 10nm (batch D) film.The solid and the dotted lines are the fit to the experimental data and the result of the two-temperature model.

Table 4.1: MgB_2 THICKNESS (d), CRITICAL TEMPERATURE (T_c), ELECTRON-PHONON INTERACTION TIME (τ_{e-ph}), PHONON ESCAPE TIME (τ_{esc}), SPECIFIC HEAT RATIO (c_e/c_{ph}) AND MIXER TIME CONSTANT (τ)

Device	d(nm)	T_c(K)	$\tau_{e-ph}(ps)$	$\tau_{esc}(ps)$	C_e/C_{ph}	$\tau(ps)$
1	30	22	7±6	42±1	1.35	130
2	15	17	12±5	12±1	2.25	70
3	10	15	11±5	9±1	3	47
4	10	8.5	15±2	6±0.2	9	106

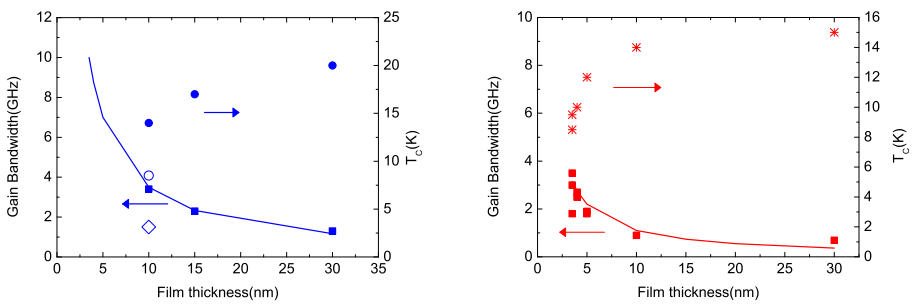

(a) (b)

Fig. 4.5: (a) The gain bandwidth (diamonds) and the critical temperature (circles) for MgB_2 HEB mixers versus the film thickness. (b) The gain bandwidth (squares) and the critical temperature (crosses) for NbN HEB mixers versus the film thickness (from ref. [75]).

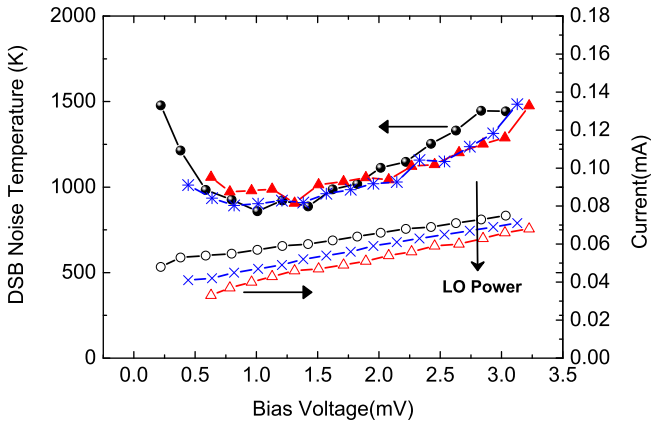

Fig. 4.6: IV curves at various LO power levels and the receiver noise temperature versus bias voltage for sample #4 at 4.2K.

extrapolated using the same GBW vs thickness dependence as for thicker film (see fig.4.5(a)). As it is possible to see from the figure 4.5(a) a GBW as large as 10 GHz can obtained with 3.5 nm thick film, which is more than twice larger than of the GBW that has been reported for NbN mixers made on 3-4 nm film.

For the noise measurements, the Y factor technique was employed to determine the receiver noise temperature. The Y factor is defined as:

$$Y = \frac{P_{out,hot}}{P_{out,cold}} = \frac{T_{rec} + T(290K)}{T_{rec} + T(77K)} \tag{4.2}$$

where hot and cold refer to two different noise sources. In particular hot is referred to the room temperature while cold to the temperature of the liquid nitrogen. The double side band (DSB) receiver noise temperature then becomes:

$$T_{rec} = \frac{T(290K) - YT(77K)}{Y - 1} \tag{4.3}$$

The I-V curves at various power levels and the DSB noise temperature versus bias voltage for device #4 are shown in figure 4.6. The receiver noise temperature had a broad band minimum around 1 mV and 60 μA. Figure 4.7 shows the noise temperature versus IF frequency in the range from 1 to 4.5 GHz and at 600 GHz LO frequency measured for device #4. Correcting for the reflection losses at the silicon lens and including noise contributions from LNA, the IR filter and beam splitter, the minimum receiver noise temperature was approximately 800 K. A noise bandwidth of 3 GHz have been extrapolated from the fit of the measured data (red solid line fig.4.7). As it was discussed previously the critical temperature of this devices was much lower compared to devices #3 and #5 also made of 10 nm film. A 20% reduction of the receiver noise temperature was observed with the reduction of the bath temperature. Indeed at 2 K the critical current of the device #4 increased from 160 μA to

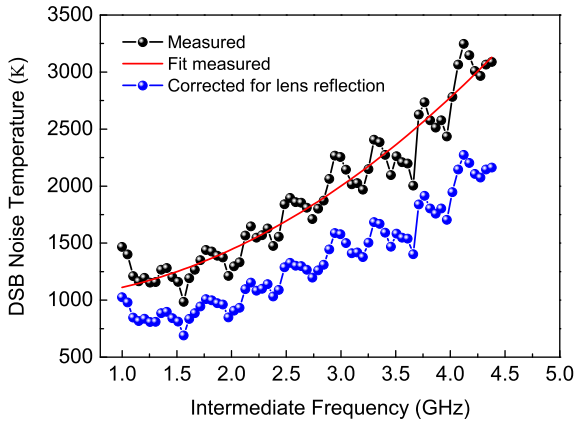

Fig. 4.7: Receiver DSB noise temperature versus IF for sample #4 at 4.2K. The solid line is a fit for a 3GHz receiver noise temperature.

$250\,\mu A$. In order to bring the mixer to the same bias point more LO power was needed and the noise temperature reduced as was discussed previously [60, 76]. The HEB mixer gain is proportional to the LO power, which explains the general tendency of HEB mixers to show an improvement in performance for lower operation temperature and higher critical temperatures. Figure 4.8

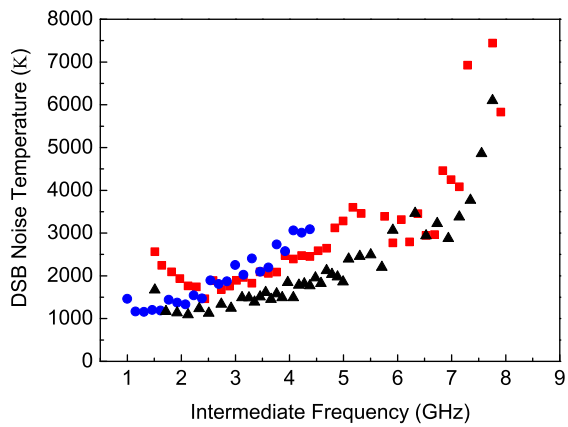

Fig. 4.8: The receiver noise temperature versus intermediate frequency. Black triangles: NbN HEB mixer at 1.9THz [28]. Blue circles: MgB_2 HEB mixer #4. Red squares: MgB_2 HEB mixer #4. Bath temperature 4.2K

.

shows the DSB noise temperature versus intermediate frequency for device #4 and #5. In the same plot, the noise spectra of HEB mixer of 3-4 nm NbN film [28] are showed for comparison reason. The noise temperature for mixer

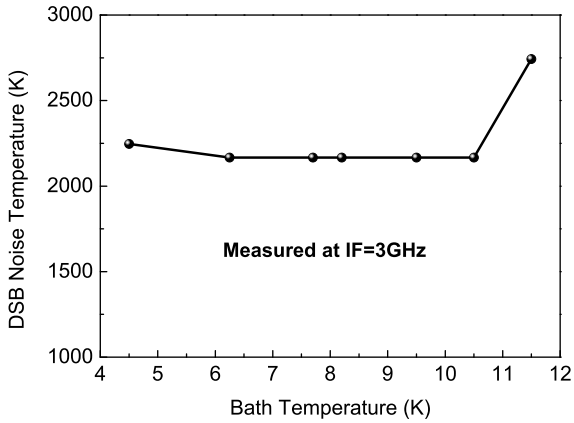

Fig. 4.9: Receiver noise temperature versus bath temperature of MgB_2 mixer #5

.

#1 to #3 was not measured indeed due to the large device area there was a lack of the LO power. For MgB_2 films with T_c larger than 15 K a submicrometer size is needed to reduce the LO power requirement to the practical values. The noise bandwidth (NBW) appeared to be more than twice larger in mixer #5 than mixer #4. The NBW extrapolated from the fit to the measured data was 6.5 GHz in mixer #5. The noise temperature of NbN HEB mixers was reported to be sensitive to the bath temperature [28,77], increasing almost immediately as the bath temperature rises. Mixer #5, has a T_c of 15 K. Therefore, it was interesting to verify how sensitive the noise temperature of such devices is to the bath temperature. As it can be observed from figure 4.9, the T_{rec} of this device (measured at IF of 3 GHz) remain constant from 4.2 K up to 10.5 K, and rising at higher temperatures.

4.3 Two-temperature model

In order to understand the physical parameters (thickness and T_c of the MgB_2 film, electron-phonon time, phonon escape time and phonon specific heats) that determine the bolometer response time and consequently the GBW the two temperature approach presented in [78] was used. The effect of the self-heating electrothermal feedback is taken in account. The HEB photo response as a function of the modulation frequency is:

$$\Delta\Theta_{IF}(\omega) \propto U_{IF}(\omega) \propto \frac{\Delta\Theta(0)C_0}{\psi(\omega) + \frac{R_0 - R_L}{R_0 + R_L}C_0} \tag{4.4}$$

$$\psi(\omega) = \frac{(1 + j\omega\tau_1)(1 + j\omega\tau_2)}{(1 + j\omega\tau_0)} \tag{4.5}$$

$$\tau_0^{-1} = \tau_{esc}^{-1} + \tau_{eph}^{-1}\frac{c_e}{c_{ph}} \tag{4.6}$$

$$\tau_{1,2}^{-1} = \frac{\tau_{esc}^{-1} + \tau_{eph}^{-1}\left(\frac{C_e}{C_{ph}} + 1\right)}{2} \times \times \left[1 \pm \left(1 - 4\frac{(\tau_{esc}^{-1} + \tau_{eph}^{-1}(C_e/C_{ph} + 1))^{-2}}{\tau_{esc}\tau_{eph}}\right)^{1/2}\right] \quad (4.7)$$

The electron specific heat is given by:

$$c_e(T_e) = \gamma T_e \quad (4.8)$$

The general approach is that at the given mixer bath temperature, the LO power and the bias voltage are optimized for the maximum mixer gain. Under such conditions, the electron temperature T_e rises close to the T_C due to the dissipation of the LO and the DC power. The electron phonon specific heat coefficient value, γ was taken from the literature. The published value of γ is in the range from 3 to 5.5 mJ/mol K^2 [79–81]. The phonon specific heat, c_{ph} was calculated using the Debye approximation (eq. 4.9) [82]. The phonon temperature T_{ph} is $\sim 0.9 \times T_e$ estimated from the heat balance equation [81].

$$c_{ph}(T_{ph}) = 9n_a K_B \left[\frac{T_{ph}}{T_D}\right]^3 \int_0^{\frac{T_D}{T_{ph}}} \frac{e^x x^4}{(e^x - 1)^2}\,\mathrm{d}x \quad (4.9)$$

Where $n_a = 3.54 \times 10^{22}$ cm^{-3} is the atomic mass density in MgB_2 calculated from the mass density ρ_m=2.7 g/cm^3 [79, 80] and the molar mass M=45.925 g/mol of MgB_2. The Debye temperature, T_D in MgB_2 was experimentally obtained to be much larger compared to other intermetallic as well as cuprate superconductors: from 700 K to 1000 K [79–81]. Using the electron-phonon interaction time and the phonon escape time as fitting parameters, the two temperature model was applied to the gain bandwidth measured data. The dashed curves in the plots of the intermediate frequency response (figures 4.3 and 4.4) represent the fit of the 2T model. Table 4.1 shows a summary of the electron phonon interaction time, the phonon escape time and the specific heat ratio (c_e/c_{ph}) for different MgB_2 film thicknesses (30, 15 and 10 nm) given by the 2T model applied to the experimental results. For thinner films the electron-phonon interaction time and the specific heat ratio increases due to the lower critical temperature. The phonon-escape time decreases proportionally to the film thickness. The electron-phonon interaction time is a function of the temperature, $\tau_{e-ph} \propto T^{-\mu}$.

Figure 4.10 shows the electron-phonon interaction time versus the critical temperature. The 2T model has confirmed that at lower critical temperature the electron phonon interaction time increases. The open circles are for the electron phonon time extrapolated from the two temperature model (see table 4.1) whereas the open triangle is the value reported in literature ($\tau_{e-ph} = 3ps$) for a critical temperature as high as 40 K [46]. The data of the figure 4.10 were fitted using equation equation, $\tau_{e-ph} \propto T^{-\mu}$ with $\mu \approx 1.08$. Figure 4.11 shows the electron and phonon specific heats (c_e,c_{ph}) and the specific heat ratio (c_e,c_{ph}) extrapolated from the 2T model (see Table 4.1) as a function of the critical temperature. The specific heat ratio is an important factor

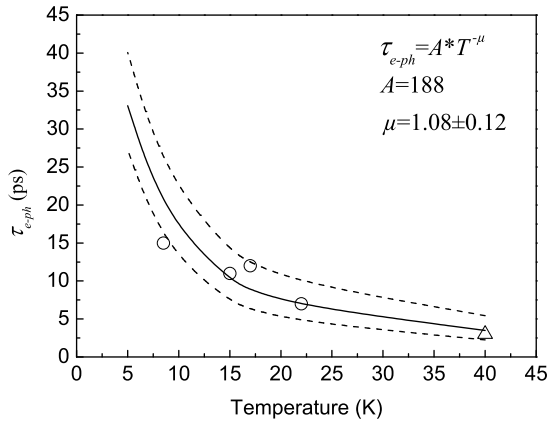

Fig. 4.10: Electron-phonon interaction time in MgB_2 as a function of the temperature, obtained from the gain bandwidth measurements and the 2T-model analysis. Open circles: this work; the triangle: from the literature. The solid line is the fit to the data (the exact formula is given in the inset). The dashed lines show the estimated error margins

.

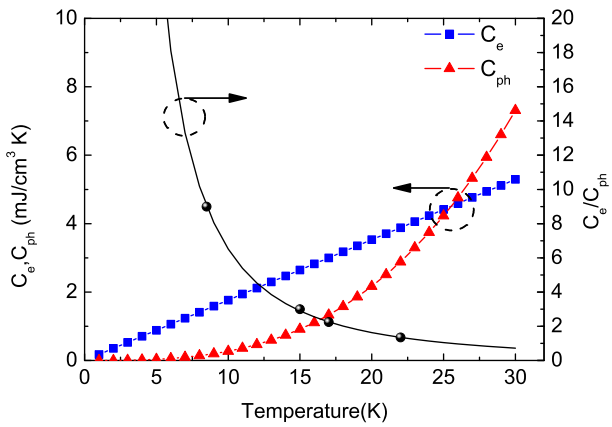

Fig. 4.11: Electron and phonon specific heats and the specific heat ratio as a function of the temperature for MgB_2. The c_e/c_{ph} ratio is plotted for the electron temperature equal to the phonon temperature. Filled circles indicate c_e/c_{ph} at the critical temperature of the films used in this work.

.

together with the electron-phonon interaction time and the phonon escape time in the system response. Indeed in order to achieve a short relaxation time all of these parameters must be optimized. Within the 2T model, it has been demonstrated that the phonon-cooled HEB mixer requires a film with a high critical temperature T_c to minimize the electron phonon interaction time

and the specific heat ratio. On the other hand, to ensure fast removal of the energy from the phonons, the film thickness should be small.

The larger GBW measured in device #3 compared to device #4 can also be explained in the frame of the 2T model. As it is possible to see from the Table 4.1, the electron phonon interaction time is larger in device #4, furthermore the specific heat ratio is also three times higher in device #4 with the consequence of a larger relaxation time and smaller GBW than device #3. Larger GBW is expected for very thin MgB_2 film with a high T_c.

Chapter 5

Conclusions and future work

In this thesis, novel THz mixers made from magnesium diboride film were fabricated, characterised and analysed using the two temperature model. The oxidation issues of the MgB_2 film leaded to important challenges during the HEB fabrication in order to achieve a high yield and a reproducible process. The motivation of this research was to study and analyze new superconducting HEB mixers with the aim to achieve better performances than other HEB mixers e.g. NbN HEB mixers.

The gain bandwidth and noise measurements were performed with 600 GHz local oscillator frequency. The gain bandwidth was investigated respect to the film thickness and the critical temperature. Several devices were fabricated in 30 nm, 15 nm and 10 nm MgB_2 film with gain bandwidths of 1.3, 2.3 and 3.4 GHz and energy relaxation times of 130, 70 and 47 ps, respectively. Moreover, by applying the two temperatures model to the measured gain bandwidth data, the electron-phonon interaction time, τ_{e-ph} of 7 to 15 ps, the phonon escape time, τ_{esc} of 6 to 42 ps and the specific heat ratio, c_e/c_{ph} of 1.35 to 9 were deduced for the given MgB_2 film thicknesses. The noise bandwidth of a mixer made of 10 nm film with a critical temperature of 15K was 6-7 GHz which is close to the one reported for HEB mixers made of 3-4 nm NbN films. The corresponding receiver noise temperature was 1500 K at 600 GHz. A receiver noise temperature of 600 K was measured at 2 K bath temperature and 600 GHz local oscillator frequency for devices fabricated in 10 nm film with a critical temperature as high as 8.5 K. In the same devices the noise temperature was measured to be 800 K at 4.2 K bath temperature.

Further development of the MgB_2 HEB mixers will require even thinner films with higher critical temperature. In fact, for very thin films and a high critical temperature the electron relaxation time is reduced and the gain bandwidth is improved. Figure 5.1 shows the extrapolation of a gain bandwidth of 8-10 GHz from the two temperature model for thin film (7.5-10nm) with high critical temperature (30-34K). Optimisation of the film deposition process will require to keep high critical temperature in films in which the thickness is a few lattice constants. Moreover, further improvements of the MgB_2 HEB mixers can be achieved in bolometer with submicrometer sizes.

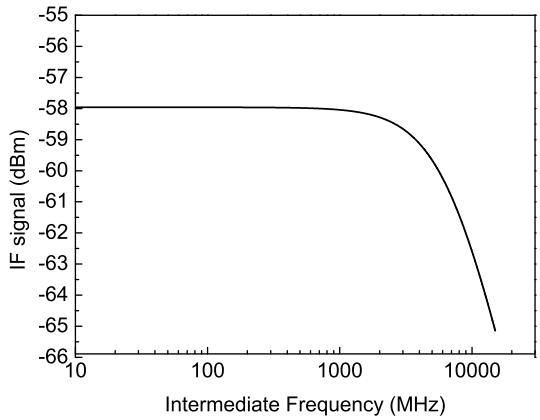

Fig. 5.1: From the two temperature model a gain bandwodth of 8-10GHz is extrapolated for film as thin as 7.5-10nm with a critical temperature as high as 30-34K

Study of the MgB_2 films, in particular specific heat measurements in a wide temperature range will allow to obtain information about important material parameters such us the electronic specific heat coefficient and the Debye temperature which will enable better accuracy for bolometer model.

Based on this research MgB_2 thin films appear very promising for low noise and wide gain bandwidth mixers for THz radio astronomy, as well as in other applications requiring broadband THz mixers.

Chapter 6

Summary of appended papers

This chapter presents a summary of the appended papers and a short description of my contribution for each paper.

Paper A

Investigation of MgB_2 HEB mixer gain bandwidth

Preliminary gain bandwidth data for HEBs made on different MgB_2 film thickness are reported. I personally contribute with: design and processing of HEBs, measurements, analysis of the data and writing. The gain bandwidth measurements were performed with help of my supervisor Sergey Cherednichenko.

Paper B

Low noise MgB2 terahertz hot-electron bolometer mixers

In this paper, a noise temperature of 600K measured at 2K and 0.6THz using HEBs made of 10nm MgB_2 films is presented. I personally contributed with: design and processing of HEBs, measurements and analysis of the data. The noise measurements were performed with help of my supervisor Sergey Cherednichenko.

Paper C

Study of IF bandwidth of MgB_2 phonon-cooled Hot electron bolometer mixers

In this paper, results of the noise and gain bandwidth investigation using HEB mixers made of 10nm MgB_2 film with a critical temperature as high as 15K are reported. I personally contribute with: design and processing of HEBs, measurements, analysis of the data and writing. The RF measurements were performed with help of my supervisor Sergey Cherednichenko.

Acknowledgment

During this time I have worked with a number of people with in some way or another have made important contribution to my work. First of all, I am indebted to my supervisor Assoc. Prof. Sergey Cherednichenko whom knowledge, guidance and advices have been very important to me. I would like to say thanks to him for pushing me in the right direction. Thank to my examiner and co-supervisor Professor Jan Stake for his support and for giving me the possibility to start the PhD at the Terahertz and Millimetre Wave Laboratory. Many special thanks to Vladimir Drakinskiy for the fruitful discussions, for his advices and help in the process lab and for proofreading the thesis. In addition, I want to thank Assoc. Prof. Josip Vukusic for introducing me in the Terahertz and Millimetre Wave Laboratory and for giving me some hints about the processing and Prof. Erik Kollberg for proofreading the thesis.

Hiroyuki Shibata and Professor Yasuhiro Tokura from NTT Basic Research Laboratories, are acknowledged for the material grown and for proofreading the papers.

I am grateful to Dr. Per-Åke Nilsson for introducing me the fabrication techniques before I started my PhD studies. Thanks to all my colleagues at TML for the friendly atmosphere that has been created. In particular Omid Habibpour, Aik Yean Tang and Aleksandra Malko.

I want to thank all the staff of the Nanofabrication Laboratory, in particular: John Halonen, Henrik Fredriksen, Kaija Matikainen, Mahdad Sadeghi and Bengt Nilsson.

Special thanks to my big family for their love and support especially during these years far from home. Finally, I owe everything to my fiancé Giuseppe for his encouraging and infinite support and patience. To you and my parents I dedicate this thesis.

This work was financially supported by the Swedish Research Council (VR) and the Swedish National Space Board.

Bibliography

[1] P. Siegel, "Terahertz technology," *IEEE Transactions on Microwave Theory and Techniques*, vol. 50, no. 3, pp. 910–928, mar 2002.

[2] ——, "Terahertz technology in biology and medicine," *IEEE Transactions on Microwave Theory and Techniques*, vol. 52, no. 10, pp. 2438–2447, oct 2004.

[3] A. Wootten and A. Thompson, "The Atacama Large Millimeter/Submillimeter Array," *Proceedings of the IEEE*, vol. 97, no. 8, pp. 1463 –1471, aug. 2009.

[4] J. Kumagal, "Space mountain submillimeter radio telescopes," *IEEE Spectrum*, vol. 42, no. 12, pp. 12 – 14, dec. 2005.

[5] D. Doyle, G. Pilbratt, and J. Tauber, "The Herschel and Planck Space Telescopes," *Proceedings of the IEEE*, vol. 97, no. 8, pp. 1403 –1411, aug. 2009.

[6] P. Richards, "Cosmic Microwave Background experiments-past, present and future," in *Infrared and Millimeter Waves, 2007 and the 2007 15th International Conference on Terahertz Electronics. IRMMW-THz. Joint 32nd International Conference on*, sept. 2007, pp. 12 –15.

[7] H.-W. Hübers, "Terahertz Heterodyne Receivers," *IEEE Journal of Selected Topics in Quantum Electronics*, vol. 14, no. 2, pp. 378–391, march-april 2008.

[8] Q. Cheng, S. Paradis, T. Bui, and M. Almasri, "Design of Dual-Band Uncooled Infrared Microbolometer," *Sensors Journal, IEEE*, vol. 11, no. 1, pp. 167–175, jan. 2011.

[9] S. Mbarek, T. Baron, S. Euphrasie, L. Thiery, B. Cretin, P. Vairac, D. Briand, J. Guillet, R. Adam, L. Chusseau, and A. Penarier, "Investigations of room temperature bolometers for THz applications," in *35th International Conference on Infrared Millimeter and Terahertz Waves (IRMMW-THz), 2010*, sept. 2010, pp. 1–2.

[10] T. Hwang, Lai, S. E. Schwarz, and D. B. Rutledge, "Microbolometers for infrared detection," *Applied Physics Letters*, vol. 34, no. 11, pp. 773 –776, jun 1979.

[11] J. Choi, V. Mitin, R. Ramaswamy, V. Pogrebnyak, M. Pakmehr, A. Muraviev, M. Shur, J. Gill, I. Mehdi, B. Karasik, and A. Sergeev, "THz Hot-Electron Micro-Bolometers Based on Low-Mobility 2DEG in GaN Heterostructures," *IEEE Sensors Journal*, vol. PP, no. 99, p. 1, 2012.

[12] P. Khosropanah, J. R. Gao, W. M. Laauwen, M. Hajenius, and T. M. Klapwijk, "Low noise NbN hot electron bolometer mixer at 4.3 THz," *Applied Physics Letters*, vol. 91, no. 22, pp. 221 111 –221 111–3, nov 2007.

[13] W. Zhang, P. Khosropanah, J. R. Gao, E. L. Kollberg, K. S. Yngvesson, T. Bansal, R. Barends, and T. M. Klapwijk, "Quantum noise in a terahertz hot electron bolometer mixer," *Applied Physics Letters*, vol. 96, no. 11, pp. 111 113–111 113–3, mar 2010.

[14] Y. Lobanov, E. Tong, R. Blundell, A. Hedden, B. Voronov, and G. Gol'tsman, "Large-Signal Frequency Response of an HEB Mixer: From 300 MHz to Terahertz," *IEEE Transactions on Applied Superconductivity*, vol. 21, no. 3, pp. 628 –631, june 2011.

[15] W. Zhang, W. Miao, K. Zhou, S. Li, Z. Lin, Q. Yao, and S. Shi, "Heterodyne Mixing and Direct Detection Performance of a Superconducting NbN Hot-Electron Bolometer," *IEEE Transactions on Applied Superconductivity*, vol. 21, no. 3, pp. 624–627, june 2011.

[16] B. Karasik, D. Olaya, J. Wei, S. Pereverzev, M. Gershenson, J. Kawamura, W. McGrath, and A. Sergeev, "Record-Low NEP in Hot-Electron Titanium Nanobolometers," *IEEE Transactions on Applied Superconductivity*, vol. 17, no. 2, pp. 293–297, june 2007.

[17] W. Shan, J. Yang, S. Shi, Q. Yao, Y. Zuo, Z. Lin, S. Chen, X. Zhang, W. Duan, A. Cao, S. Li, Z. Li, J. Liu, and J. Zhong, "Development of Superconducting Spectroscopic Array Receiver: A Multibeam 2SB SIS Receiver for Millimeter-Wave Radio Astronomy," *IEEE Transactions on Terahertz Science and Technology*, vol. PP, no. 99, pp. 1–12, november 2012.

[18] B. Jackson and T. Klapwijk, "The current status of low-noise thz mixers based on sis junctions," *Physica C: Superconductivity*, no. 0, pp. 368 – 373, 2002.

[19] X.-F. Shen, X.-S. Cao, J. Li, and S.-C. Shi, "Comparison of the THz Direct-Detection Behaviors of Nb and NbN Superconducting Tunnel Junctions," in *Global Symposium on Millimeter Waves, GSMM 2008.*, april 2008, pp. 94 –97.

[20] D. Schoenherr, C. Bleasdale, T. Goebel, C. Sydlo, H. Hartnagel, R. Lewis, and P. Meissner, "Extremely broadband characterization of a Schottky diode based THz detector," in *35th International Conference on Infrared Millimeter and Terahertz Waves (IRMMW-THz), 2010*, sept. 2010, pp. 1–2.

[21] A. Maestrini, B. Thomas, H. Wang, C. Jung, J. Treuttel, Y. Jin, G. Chattopadhyay, I. Mehdi, and G. Beaudin, "Schottky diode-based terahertz

frequency multipliers and mixers," *Comptes Rendus Physique*, vol. 11, pp. 480 – 495, 2010.

[22] F. Zhong, B. Zhang, Y. Fan, M. Zhao, and X. Yang, "A Broadband W-band Subharmonic Mixers Circuit Based on Planar Schottky Diodes," in *International Conference on Industrial Control and Electronics Engineering (ICICEE), 2012*, aug. 2012, pp. 792–794.

[23] A. Lisauskas, S. Boppel, D. Seliuta, L. Minkevicius, I. Kasalynas, G. Valusis, V. Krozer, and H. G. Roskos, "Terahertz detection and coherent imaging from 0.2 to 4.3 THz with silicon CMOS field-effect transistors," in *Microwave Symposium Digest (MTT), 2012 IEEE MTT-S International*, june 2012, pp. 1–3.

[24] R. Tauk, F. Teppe, S. Boubanga, D. Coquillat, W. Knap, Y. M. Meziani, C. Gallon, F. Boeuf, T. Skotnicki, C. Fenouillet-Beranger, D. K. Maude, S. Rumyantsev, and M. S. Shur, "Plasma wave detection of terahertz radiation by silicon field effects transistors: Responsivity and noise equivalent power," *Applied Physics Letters*, vol. 89, no. 25, pp. 253 511 –253 511–3, dec 2006.

[25] B. Ellison, B. Maddison, C. Mann, D. Matheson, M. Oldfield, S. Marazita, T. Crowe, P. Maaskant, and W. Kelly, "First Results for a 2.5 THz Schottky Diode Waveguide Mixer," in *Seventh International Symposium on Space Terahertz Technology*, Mar. 1996, p. 494.

[26] D. Winkler and T. Claeson, "High-frequency limits of superconducting tunnel junction mixers," *Journal of Applied Physics*, vol. 62, no. 11, pp. 4482–4498, 1987.

[27] G. de Lange, J. J. Kuipers, T. M. Klapwijk, R. A. Panhuyzen, H. van de Stadt, and M. W. M. de Graauw, "Superconducting resonator circuits at frequencies above the gap frequency," *Journal of Applied Physics*, vol. 77, no. 4, pp. 1795 –1804, feb 1995.

[28] S. Cherednichenko, V. Drakinskiy, T. Berg, P. Khosropanah, and E. Kollberg, "Hot-electron bolometer terahertz mixers for the Herschel Space Observatory," *Review of Scientific Instruments*, vol. 79, no. 3, pp. 034 501 –034 501–10, mar 2008.

[29] P. Lehikoinen, J. Mallat, P. Piironen, A. Lehto, J. Tuovinene, and A. V. Räisänen, "A 119 GHz planar Schottky diode mixer for a space application," *International Journal of Infrared and Millimeter Waves*, vol. 17, pp. 807–818, 1996.

[30] P. Siegel, R. Dengler, I. Mehdi, W. Bishop, and T. Crowe, "A 200 GHz planar diode subharmonically pumped waveguide mixer with state-of-the-art performance," in *Microwave Symposium Digest, 1992., IEEE MTT-S International*, jun 1992, pp. 595–598 vol.2.

[31] B. Thomas, A. Maestrini, and G. Beaudin, "A low-noise fixed-tuned 300-360 GHz sub-harmonic mixer using planar Schottky diodes," *Microwave and Wireless Components Letters, IEEE*, vol. 15, no. 12, pp. 865–867, dec 2005.

[32] K. Hui, J. Hesler, D. Kurtz, W. Bishop, and T. Crowe, "A micromachined 585 GHz Schottky mixer," *Microwave and Guided Wave Letters, IEEE*, vol. 10, no. 9, pp. 374 –376, sep 2000.

[33] W. Bishop, K. McKinney, R. Mattauch, T. Crowe, and G. Green, "A Novel Whiskerless Schottky Diode for Millimeter and Submillimeter Wave Application," in *Microwave Symposium Digest, 1987 IEEE MTT-S International*, vol. 2, 9 1975-june 11 1987, pp. 607–610.

[34] B. Thomas, P. G. Huggard, B. Alderman, B. P. Moyna, M. L. Oldfield, B. N. Ellison, and D. N. Matheson, "Integrated Heterodyne Receivers for MM SubMM Atmospheric Remote Sensing," in *MM-Wave Products and Technologies, 2006. The Institution of Engineering and Technology Seminar on*, nov. 2006, pp. 13 –18.

[35] P. Sobis, N. Wadefalk, A. Emrich, and J. Stake, "A Broadband, Low Noise, Integrated 340 GHz Schottky Diode Receiver," *IEEE Microwave and Wireless Components Letters*, vol. 22, no. 7, pp. 366–368, 2012.

[36] F. Arams, C. Allen, B. Peyton, and E. Sard, "Millimeter mixing and detection in bulk InSb," *Proceedings of the IEEE*, vol. 54, no. 4, pp. 612–622, april 1966.

[37] K. S. Yngvesson, J.-X. Yang, F. Agahi, D. Dai, C. Musante, W. Grammer, and K. M. Lau, "AlGaAs/GaAs quasi-bulk effect mixers: Analysis and experiments," in *Third International Symposium on Space Terahertz Technology*, 1992, pp. 688–705.

[38] M. Kroug, S. Cherednichenko, H. Merkel, E. Kollberg, B. Voronov, G. Gol'tsman, H. Huebers, and H. Richter, "NbN hot electron bolometric mixers for terahertz receivers," *IEEE Transactions on Applied Superconductivity*, vol. 11, no. 1, pp. 962–965, mar 2001.

[39] J. W. Kooi, J. J. A. Baselmans, M. Hajenius, J. R. Gao, T. M. Klapwijk, P. Dieleman, A. Baryshev, and G. de Lange, "IF impedance and mixer gain of NbN hot electron bolometers," *Journal of Applied Physics*, vol. 101, no. 4, pp. 044 511–044 511–8, feb 2007.

[40] A. Skalare, W. R. McGrath, B. Bumble, H. G. LeDuc, P. J. Burke, A. A. Verheijen, R. J. Schoelkopf, and D. E. Prober, "Large bandwidth and low noise in a diffusion-cooled hot-electron bolometer mixer," *Applied Physics Letters*, vol. 68, no. 11, pp. 1558–1560, mar 1996.

[41] I. Tretyakov, S. Ryabchun, M. Finkel, A. Maslennikova, K. N., A. Lobastova, B. Voronov, and G. Gol'tsman, "Low noise and wide bandwidth of NbN hot-electron bolometer mixers," *Applied Physics Letters*, vol. 98, no. 3, pp. 033 507–3, 2011.

[42] D. E. Prober, "Superconducting terahertz mixer using a transition-edge microbolometer," *Applied Physics Letters*, vol. 62, no. 17, pp. 2119 –2121, apr 1993.

[43] J. Nagamatsu, N. Nakagawa, T. Muranaka, Y. Zenitani, and J. Akimitsu, "Superconductivity at 39 K in magnesium diboride," *Nature*, vol. 410, no. 6824, pp. 63–64, feb 2001.

[44] J. Baselmans, A. Baryshev, S. Reker, M. Hajenius, J. Gao, T. Klapwijk, B. Voronov, and G. Gol'tsman, "Influence of the direct response on the heterodyne sensitivity of hot electron bolometer mixers," *Journal of Applied Physics*, vol. 100, no. 8, pp. 084 510–7, 2006.

[45] Z. Yuhao, L. Zhiyuan, D. Qian, L. Dongyao, W. Yinbo, Z. Yan, W. Yue, and F. Qingrong, "Ultrathin MgB_2 films fabricated on Al_2O_3 substrate by hybrid physical chemical vapor deposition with high Tc and Jc," *Superconductor Science and Technology*, vol. 24, no. 1, jan 2011.

[46] Y. Xu, M. Khafizov, L. Satrapinsky, P. Kúš, A. Plecenik, and R. Sobolewski, "Time-Resolved Photoexcitation of the Superconducting Two-Gap State in MgB_2 Thin Films," *Phys. Rev. Lett.*, vol. 91, p. 197004, Nov 2003.

[47] K. S. Ilin, M. Lindgren, M. Currie, A. D. Semenov, G. N. Goltsman, R. Sobolewski, S. I. Cherednichenko, and E. M. Gershenzon, "Picosecond hot-electron energy relaxation in NbN superconducting photodetectors," *Applied Physics Letters*, vol. 76, no. 19, pp. 2752 –2754, may 2000.

[48] A. Rogalski and F. Sizov, "Terahertz detectors and focal plane arrays," *Opto-Electronics Review*, vol. 19, pp. 346–404, Sep. 2011.

[49] P. L. Richards, "Bolometers for infrared and millimeter waves," *Journal of Applied Physics*, vol. 76, no. 1, pp. 1–24, jul 1994.

[50] A. J. Miller, A. Luukanen, and E. N. Grossman, "Micromachined antenna-coupled uncooled microbolometers for terahertz imaging arrays," pp. 18–24, 2004.

[51] J. B. Johnson, "Thermal Agitation of Electricity in Conductors," *Phys. Rev.*, vol. 32, pp. 97–109, Jul 1928.

[52] J. W. Zhou, K. Farooqui, P. Timbie, G. Wilson, C. Allen, S. Moseley, and D. Mott, "Monolithic silicon bolometers as sensitive MM wave detectors," in *Microwave Symposium Digest, 1995., IEEE MTT S International*, vol. 3, may 1995, pp. 1347 –1350.

[53] B. Karasik, D. Olaya, J. Wei, S. Pereverzev, M. Gershenson, J. Kawamura, W. McGrath, and A. Sergeev, "Record-Low NEP in Hot-Electron Titanium Nanobolometers," *IEEE Transactions on Applied Superconductivity*, vol. 17, pp. 293–297, Jun. 2007.

[54] E. Gershenzon, G. Gol´tsman, I. Gogidze, Y. Gusev, A. Elantev, B. Karasik, and A. Semenov, "Millimeter and submillimeter range mixer based on electronic heating of superconductive films in the resistive state," *Superconductivity*, vol. 10, no. 3, pp. 1582–1597, 1990.

[55] K. Yngvesson and E. Kollberg, "Optimum Receiver Noise Temperature for NbN HEB Mixers According to the Standard Model," in *Tenth International Symposium on Space Terahertz Technology*, T. Crowe and R. Weikle, Eds., Mar. 1999, p. 563.

[56] H. Ekstrom, E. Kollberg, P. Yagoubov, G. Goltsman, E. Gershenzon, and S. Yngvesson, "Gain and noise bandwidth of NbN hot-electron bolometric mixers," *Applied Physics Letters*, vol. 70, no. 24, pp. 3296 –3298, jun 1997.

[57] J. Zmuidzinas and P. Richards, "Superconducting detectors and mixers for millimeter and submillimeter astrophysics," *Proceedings of the IEEE*, vol. 92, no. 10, pp. 1597 – 1616, oct. 2004.

[58] T. G. Phillips and K. B. Jefferts, "A Low Temperature Bolometer Heterodyne Receiver for Millimeter Wave Astronomy," *Review of Scientific Instruments*, vol. 44, no. 8, pp. 1009–1014, aug 1973.

[59] A. D. Semenov, H. Richter, H.-W. Hubers, B. Gunther, A. Smirnov, K. S. Il'in, M. Siegel, and J. P. Karamarkovic, "Terahertz Performance of Integrated Lens Antennas With a Hot-Electron Bolometer," *IEEE Transactions on Microwave Theory and Techniques*, vol. 55, no. 2, pp. 239 –247, feb. 2007.

[60] B. S. Karasik and A. I. Elantiev, "Noise temperature limit of a superconducting hot electron bolometer mixer," *Applied Physics Letters*, vol. 68, no. 6, pp. 853–855, feb 1996.

[61] A. Sergeev and V. Mitin, "Electron-phonon interaction in disordered conductors: Static and vibrating scattering potentials," *Phys. Rev. B*, vol. 61, pp. 6041–6047, Mar 2000.

[62] B. Karasik, A. Sergeev, and D. Prober, "Nanobolometers for THz Photon Detection," *IEEE Transactions on Terahertz Science and Technology*, vol. 1, no. 1, pp. 97–111, sept. 2011.

[63] J. R. Waldram, *Superconductivity of Metals and Cuprates.* Institute of Physics Publishing, 1996.

[64] J. R. Gavaler, M. A. Janocko, and C. K. Jones, "Preparation and properties of high-Tc Nb_3Ge films," *Journal of Applied Physics*, vol. 45, no. 7, pp. 3009 –3013, jul 1974.

[65] B. Cristina and Y. Tsutomu, "Review of the superconducting properties of MgB_2," *Superconductor Science and Technology*, vol. 14, no. 11, nov 2001.

[66] XXXi, "MgB_2 thin films," *Superconductor Science and Technology*, vol. 22, no. 4, apr 2009.

[67] S. Cherednichenko, P. Khosropanah, E. Kollberg, M. Kroug, and H. Merkel, "Terahertz superconducting hot-electron bolometer mixers," *Physica C: Superconductivity*, vol. 372-376, Part 1, no. 0, pp. 407–415, 2002.

[68] Y. Cui, J. Jones, A. Beckley, R. Donovan, D. Lishego, E. Maertz, A. Pogrebnyakov, P. Orgiani, J. Redwing, and X. Xi, "Degradation of MgB_2 thin films in water," *IEEE Transactions on Applied Superconductivity*, vol. 15, no. 2, pp. 224 – 227, june 2005.

[69] R. K. Singh, Y. Shen, R. Gandikota, J. M. Rowell, and N. Newman, "Effect of stoichiometry on oxygen incorporation in mgb2 thin films," 2007.

[70] H. Shibata, H. Takesue, T. Honjo, T. Akazaki, and Y. Tokura, "Single-photon detection using magnesium diboride superconducting nanowires," *Applied Physics Letters*, vol. 97, no. 21, pp. 212 504–212 504–3, nov 2010.

[71] K. Ueda and M. Naito, "In situ growth of superconducting MgB_2 thin films by molecular-beam epitaxy," *Journal of Applied Physics*, vol. 93, no. 4, pp. 2113–2120, feb 2003.

[72] I. Mazin, O. Andersen, O. Jepsen, O. Dolgov, J. Kortus, A. Golubov, A. Kuz'menko, and D. M. van der, "Superconductivity in MgB_2: Clean or Dirty?" *Physical Review Letters*, vol. 89, no. 10, pp. 107 002/1–107 002/4, 2002.

[73] http://www.eccosorb.com/.

[74] H. Ekström, B. Karasik, E. Kollberg, and K. Yngvesson, "Conversion gain and noise of niobium superconducting hot-electron-mixers," *IEEE Transactions on Microwave Theory and Techniques*, vol. 43, no. 4, pp. 938–947, apr 1995.

[75] S. Cherednichenko, P. Yagoubov, K. Il'in, G. Gol'tsman, and E. Gershenzon, "Large Bandwidth of NbN Phonon-Cooled Hot-Electron Bolometer Mixers," in *27th European Microwave Conference, 1997.*, vol. 2, sept. 1997, pp. 972–977.

[76] W. Zhang, N. Li, L. Jiang, Y. Ren, Q.-J. Yao, Z.-H. Lin, S.-C. Shi, B. M. Voronov, and G. N. Gol'tsman, "Dependence of noise temperature of quasi-optical superconducting hot-electron bolometer mixers on bath temperature and optical-axis displacement," pp. 684 007–684 007–8, 2007.

[77] S. Cherednichenko, M. Kroug, H. Merkel, E. Kollberg, D. Loudkov, K. Smirnov, B. Voronov, G. Gol'Tsman, and E. Gershenzon, "Local Oscillator Power Requirement and Saturation Effects in NbN HEB Mixers," in *Twelfth International Symposium on Space Terahertz Technology*, I. Mehdi, Ed., Dec. 2001, p. 273.

[78] N. Perrin and C. Vanneste, "Response of superconducting films to a periodic optical irradiation," *Phys. Rev. B*, vol. 28, pp. 5150–5159, Nov 1983.

[79] F.-Y. Li, R.-J. Wang, S.-C. Li, L.-C. Chen, J.-L. Zhu, Z.-X. Liu, R.-C. Yu, and C.-Q. Jin, "Ultrasound studies of MgB_2 superconductor under hydrostatic pressure," *Phys. Rev. B*, vol. 65, p. 132517, Mar 2002.

[80] C. Wälti, E. Felder, C. Degen, G. Wigger, R. Monnier, B. Delley, and H. R. Ott, "Strong electron-phonon coupling in superconducting MgB_2:A specific heat study," *Phys. Rev. B*, vol. 64, p. 172515, Oct 2001.

[81] L. Jian-Lin, Z. Jie, C. Zhao-Jia, B. Hai-Yang, W. Yu-Peng, M. Ji-Bao, J. Duo, R. Zhi-An, C. Guang-Can, and Z. Zhong-Xian, "Low Temperature Specific Heat of Superconducting MgB_2," *Chinese Physics Letters*, vol. 18, no. 6, p. 820, 2001.

[82] J. S. Blakemore, *Solid State Physics (2nd ed)*. Cambridge, UK: University press, 1985.